

EDUCATIONAL REVIEW

Open Access



Multimodality imaging of neurodegenerative disorders with a focus on multiparametric magnetic resonance and molecular imaging

James Ryan Loftus* , Savita Puri and Steven P. Meyers

Abstract

Neurodegenerative diseases afflict a large number of persons worldwide, with the prevalence and incidence of dementia rapidly increasing. Despite their prevalence, clinical diagnosis of dementia syndromes remains imperfect with limited specificity. Conventional structural-based imaging techniques also lack the accuracy necessary for confident diagnosis. Multiparametric magnetic resonance imaging and molecular imaging provide the promise of improving specificity and sensitivity in the diagnosis of neurodegenerative disease as well as therapeutic monitoring of monoclonal antibody therapy. This educational review will briefly focus on the epidemiology, clinical presentation, and pathologic findings of common and uncommon neurodegenerative diseases. Imaging features of each disease spanning from conventional magnetic resonance sequences to advanced multiparametric methods such as resting-state functional magnetic resonance imaging and arterial spin labeling imaging will be described in detail. Additionally, the review will explore the findings of each diagnosis on molecular imaging including single-photon emission computed tomography and positron emission tomography with a variety of clinically used and experimental radiotracers. The literature and clinical cases provided demonstrate the power of advanced magnetic resonance imaging and molecular techniques in the diagnosis of neurodegenerative diseases and areas of future and ongoing research. With the advent of combined positron emission tomography/magnetic resonance imaging scanners, hybrid protocols utilizing both techniques are an attractive option for improving the evaluation of neurodegenerative diseases.

Key points

- Neurodegenerative diseases represent a growing substantial burden of disease worldwide.
- Clinical diagnosis and standard imaging techniques lack accuracy in diagnosing dementia syndromes.
- Multiparametric magnetic resonance and molecular imaging are tools for evaluating neurodegenerative disease.
- Combined positron emission tomography/magnetic resonance imaging protocols provide the ideal dementia appraisal.

Keywords Neurodegenerative disease, Molecular imaging, Multiparametric MRI, Alzheimer's disease, Dementia

*Correspondence:

James Ryan Loftus

James_Loftus@urmc.rochester.edu

Department of Imaging Sciences, University of Rochester Medical Center,
601 Elmwood Ave, Rochester, NY 14642, USA



© The Author(s) 2023. **Open Access** This article is licensed under a Creative Commons Attribution 4.0 International License, which permits use, sharing, adaptation, distribution and reproduction in any medium or format, as long as you give appropriate credit to the original author(s) and the source, provide a link to the Creative Commons licence, and indicate if changes were made. The images or other third party material in this article are included in the article's Creative Commons licence, unless indicated otherwise in a credit line to the material. If material is not included in the article's Creative Commons licence and your intended use is not permitted by statutory regulation or exceeds the permitted use, you will need to obtain permission directly from the copyright holder. To view a copy of this licence, visit <http://creativecommons.org/licenses/by/4.0/>.

Background

Neurodegenerative disease (NDDs) including dementia syndromes represent a substantial burden of disease worldwide. Estimated global prevalence of all-cause dementia is 700 per 100,000 persons with the number of patients with dementia nearly doubling every five years [1]. Clinical diagnosis alone remains not entirely reliable with a median sensitivity of 87% and specificity of 58% [2]. Proper diagnosis is crucial to aid with prognostication and pharmacologic management of patients with NDDs, with disease modifying therapies an active field of research interest and recent US Food and Drug Administration approval of aducanumab, an IgG1 anti-amyloid-beta antibody targeting amyloid beta plaques, the first therapy of its kind available, though not yet approved in Europe [3–6]. Imaging is often applied to increase diagnostic confidence in the setting of a suspected NDD and in 2011 the US National Institute on Aging and the Alzheimer's Association incorporated imaging biomarkers into the guidelines for diagnosis of Alzheimer's disease (AD) [7]. Structural imaging methods such as magnetic resonance imaging (MRI) are often undertaken first, though limited sensitivity and specificity and high inter-observer variability limit the applicability of these more commonly used methods [8]. Molecular imaging provides promise in its unique ability to visualize the spatial distribution of pathologic changes in NDDs and has been demonstrated to lead to increases in diagnostic certainty and provide therapeutic guidance. We aim to provide a brief review of the characteristics and epidemiology of NDDs, as this topic has been covered in detail elsewhere, and focus on their imaging features across multiple modalities, particularly advanced multiparametric MRI and molecular imaging.

Alzheimer's disease

Alzheimer's disease is the most common form of progressive dementia which accounts for up to 60% of cases in patients older than 65 years [9]. Alzheimer's disease is pathologically defined by senile gray matter plaques consisting of neurotoxic deposits of extracellular amyloid-beta (A β) 42 protein, intracellular neurofibrillary tangles (NFTs) including the three repeat (3R) and four repeat (4R) tau isoforms, and decreased neuronal density from neuronal death. Neurofibrillary changes tend to progress in an orderly manner starting in the transentorhinal cortex and progressing through the medial temporal lobes to neocortical association areas in the frontal, parietal, and occipital lobes [10, 11]. Sporadic and familial forms have been defined with approximately 10% of patients related to presenilin 1 (PSEN1), presenilin 2 (PSEN2), and APOE*E4 genes. The clinical course of Alzheimer's disease typically begins with a slow decline in memory

followed by diminishing function in language, visuospatial, and executive abilities [9, 12]. Patients typically have poor recent memory; disorientation to time and place; impaired recall, recognition, object and space perception, conversational speech, and working memory; and word retrieval difficulty.

Structural imaging in the evaluation of AD is typically performed with volumetric T1-weighted imaging. Various scales and grading systems have been studied including those evaluating atrophy of the medial temporal lobes [13, 14]. Overall, these have shown adequate sensitivity and specificity, however, are limited by interobserver variation [8]. Automated segmentation methods have also shown the ability to discriminate between AD and controls [15, 16]. Image analysis software with automated volumetric segmentation of brain regions has also shown value for the prediction of development of AD from mild cognitive impairment (MCI), a condition characterized by decline in performance on standardized neurocognitive testing, demonstrating an area under the curve between 0.6 and 0.77 [17, 18]. Structural imaging is also valuable in following patients on monoclonal anti-A β antibody therapy, as pooled analysis reported approximately 40% of patients on aducanumab develop amyloid-related imaging abnormalities (ARIA) (Fig. 1) [19].

Advanced non-molecular imaging techniques have also been researched for the diagnosis of AD. Diffusion tensor imaging (DTI) has shown decreased fractional anisotropy (FA) and increased mean diffusivity (MD) in medial temporal lobe structures including the hippocampus, parahippocampal cingulum, uncinate fasciculus, and fornix as well as the posterior cingulate cortex (PCC), splenium of the corpus callosum, and superior longitudinal fasciculus [20, 21]. Magnetization transfer imaging (MTI), which relies on the exchange of magnetization between protons bound to macromolecules and free water, is another advanced MRI biomarker for evaluating AD, with values often reported as a magnetization transfer ratio (MTR) calculated by subtracting the signal of tissue prior to the pulse sequence by the signal following the pulse sequence then dividing by the signal prior to the pulse sequence [22]. Decreased MTR has been reported in multiple brain regions in AD including the locus coeruleus (LC), hippocampus, entorhinal cortex, precuneus, and global gray matter [22–24]. The proposed mechanism of decreased MTR in the LC is loss of neuromelanin and increased free water, with the LC potentially one of the earliest structures afflicted by NFTs [25, 26]. Decreased N-acetylaspartate (NAA)/myo-inositol ratio in the PCC may predict development of AD [27]. Arterial spin labeling (ASL) has been shown to be comparable to 2-[18F]fluoro-2-deoxy-d-glucose positron emission tomography (FDG-PET) in

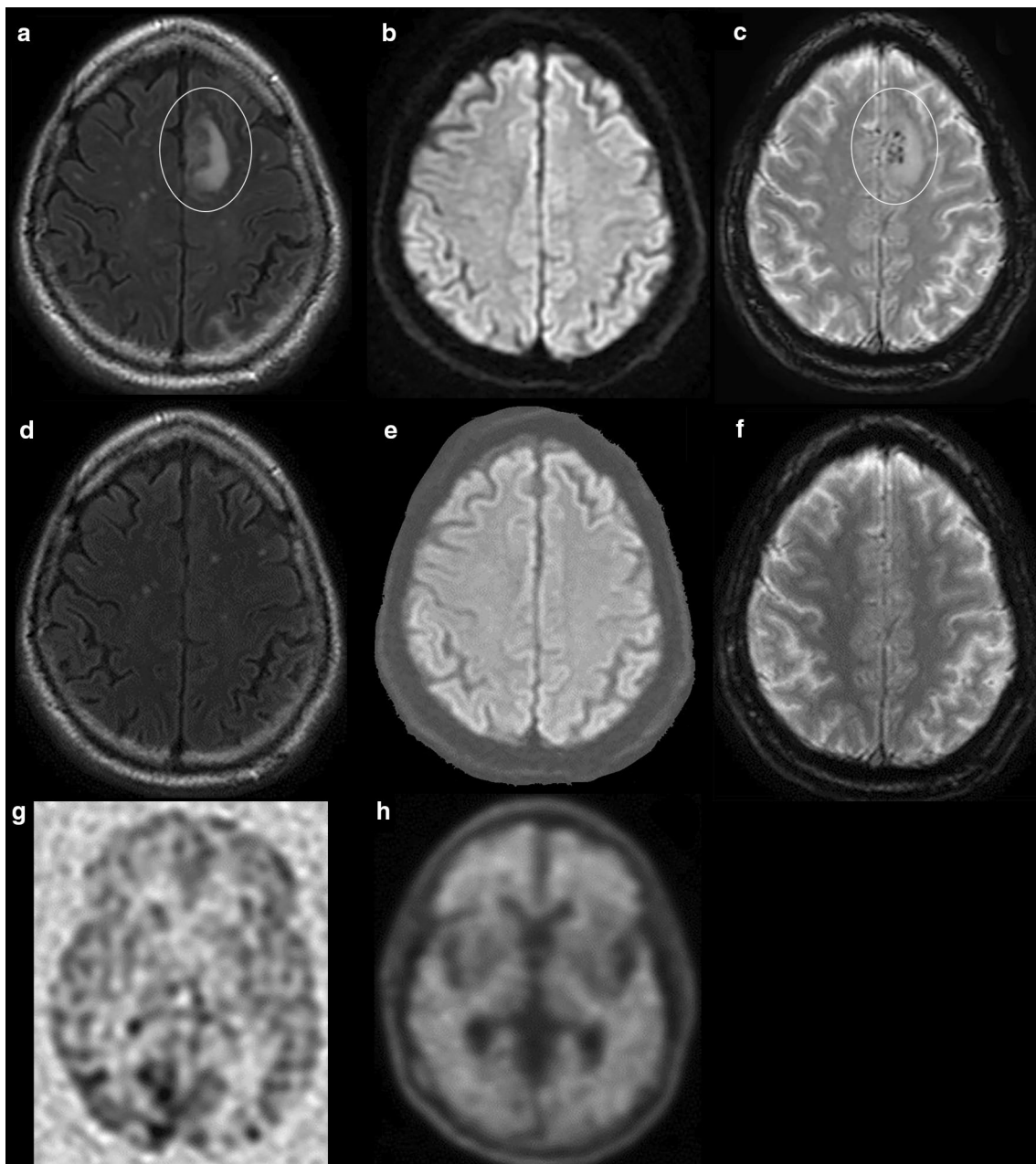


Fig. 1 A 67-year-old man with AD on anti-A β monoclonal antibody trial. T2 FLAIR image shows hyperintensity in the parasagittal left frontal lobe (oval in **a**), with no evidence of hyperintensity on DWI (**b**), and associated subcortical microhemorrhages (oval in **c**). None of these abnormalities were present prior to receiving antibody therapy (**d–f**), consistent with ARIA with edema and hemorrhage. Arterial spin labeling demonstrates hypoperfusion to the parietal and frontal lobes (**g**), with corresponding diffuse cortical uptake on florbetapir PET/CT typical of AD (**h**)

the diagnosis of AD, however, with lesser diagnostic performance in MCI [28]. Resting-state functional MRI (rsfMRI) has fairly consistently shown hypoconnectivity in the default mode network (DMN), which can be seen in earlier stages of the disease process, especially in impacted mutation carriers [29]. Decreased stiffness within the temporal and parietal lobes on magnetic resonance elastography (MRE) has been reported [30].

Recently, molecular imaging has shown promise in improving diagnostic confidence in AD. Current targets of clinically used radiotracers include glucose metabolism, amyloid beta plaques, and tau. Figure 2 demonstrates normal patterns of radiotracer activity for these agents. Patient preparation, dosing and kinetics, and normal and abnormal distribution of the commonly used radiotracers are described in Table 1.

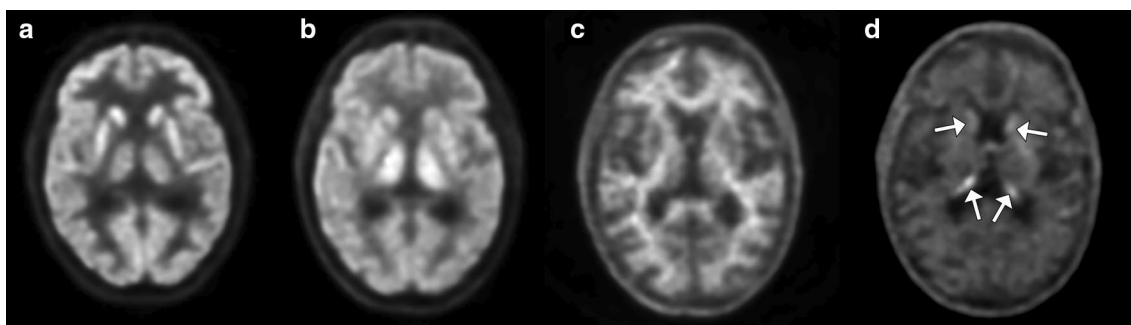


Fig. 2 Normal patterns of cerebral uptake across multiple radiotracers. Fluorodeoxyglucose PET/CT demonstrates high-grade uptake in the cortical and deep gray matter which should be greater than cerebellum (a). Cerebral blood flow imaging with early-frame or dynamic amyloid agents shows a similar pattern to FDG (b). Non-specific low-grade white matter activity with absence of gray matter activity is the normal pattern of delayed amyloid PET agents (c). Normal distribution of tau agents is low-grade gray and white matter activity with absence of elevated neocortical uptake and a variable amount of off-target binding, commonly involving the basal ganglia and choroid plexuses (arrows in d)

Fluorodeoxyglucose PET imaging has been used as a discriminatory tool for the diagnosis of AD since the early 2000s. Hypometabolism on FDG-PET scans has shown to be a reliable indicator of neuronal degeneration in AD [7]. A meta-analysis demonstrated excellent performance of FDG-PET in discriminating between AD and non-AD neurodegenerative syndromes with a sensitivity of 90% and specificity of 89% [31]. Additionally, FDG-PET has also shown signs of value in predicting the progression from amnesic type MCI to AD, especially when single-subject statistical parametric mapping (ss-SPM) was utilized, with a low probability of progression in three years with a negative study [32, 33]. Typical patterns of hypometabolism in MCI and early typical AD include the temporal lobes, parahippocampal gyri, PCC, and precuneus, with involvement of the precuneus and middle and inferior temporal gyri more characteristic of AD [34–36]. Advanced typical AD shows a fairly consistent pattern of diffuse hypometabolism involving the aforementioned areas as well as the parietal lobes and prefrontal cortex with relative sparing of the precentral gyrus, basal ganglia, and occipital cortex (Fig. 3), except in the posterior cortical atrophy (PCA, also known as Benson’s) clinical phenotype of Alzheimer’s dementia, where lateral occipital lobe atrophy and hypometabolism creates the “occipital tunnel” sign (Fig. 4) [37, 38]. Limbic-predominant AD tends to have more pronounced hypometabolism in the hippocampus and related mesial temporal lobe structures with additional involvement of the frontal cortex, while the limbic-sparing or cortical-predominant subtype involves similar regions to typical AD, with more prominent involvement of the frontal lobes and lesser involvement of the mesial temporal lobes as its name suggests [39]. Additional clinical AD phenotypes which can be discriminated on FDG-PET include the logopenic variant of primary progressive aphasia

(lvPPA) which shows left/dominant hemisphere posterior perisylvian or parietal hypometabolism and the dysexecutive/behavioral variant which has similar temporoparietal hypometabolism to typical AD however with variable involvement of the PCC and frontal lobes [40, 41].

Along with qualitative assessment, semiquantitative assessment of FDG-PET can be performed by calculating the cerebral metabolic rate of glucose (CMR_{gluc}), formally calculated by dividing the plasma glucose level by a “lumped constant,” to correct for the varying affinities of FDG and glucose for the hexokinase transporter, multiplied by the rate of transfer of FDG from blood to brain [42]. As the method is invasive and requires numerous blood draws, other methods of calculation have been developed to approximate CMR_{gluc} and standard uptake value of glucose (SUV_{gluc}) [43, 44]. Studies have linked the degree of decreased glucose metabolism with the severity of cognitive impairment on standardized mental status examinations [45, 46].

Single-subject statistical parametric mapping can also be applied to the FDG-PET data set to better quantify the degree of abnormality of an individual scan. This technique allows for voxel-based analysis through creation of a statistical map of an individual’s scan and comparing the uptake values on that scan to a series of control scans [47]. Multiple groups have documented increased diagnostic performance with ss-SPM of FDG-PET/CT [48, 49].

In comparison to FDG, A β selective radiotracers provide a disease-specific means of imaging the pathologic changes of AD in vivo. Carbon-11 (C-11) Pittsburgh compound B (PiB) was the first amyloid radiotracer used in human studies; however, the short half-life of C-11 limited its clinical applicability and fluorine-18 (F-18) labeled tracers were later produced [50]. Florbetaben (Neuraceq, Piramal, Mumbai), florbetapir (Amyvid, Eli

Table 1 Commonly used radiotracers in evaluation of neurodegenerative syndromes

	FDG-PET	Amyloid PET	Tau PET
Patient Preparation	4 to 6 h fasting Abstain from heavy exercise for 24 h prior to injection Following injection sit quietly in dimly lit room with eyes open	No special preparation	No special preparation
Administered activity MBq (mCi)	185–740 (5–20)	F-18-Florbetapir 370 (10) F-18-Florbetaben 300 (8) F-18-Flutemetamol 185 (5)	F-18-Flortaucipir 370 (10)
Effective dose	0.019 mSv/MBq	~6–7 mSv	~8–9 mSv
Uptake period (minutes)	30–60	F-18-Florbetapir 30–50 F-18-Florbetaben 45–130 F-18-Flutemetamol 90 *Note dynamic imaging immediately following bolus can also be performed to estimate cerebral blood flow	F-18-Flortaucipir 80
Acquisition time (minutes)		F-18-Florbetapir 10 F-18-Florbetaben 15–20 F-18-Flutemetamol 20	F-18-Flortaucipir 20
Normal study	Uptake within the cerebral cortex and deep gray nuclei greater than cerebellum	Uptake within the cerebral white matter	Absence of neocortical uptake. Note there can be significant off-target binding in the striatum, choroid plexus, and brainstem nuclei which is considered normal
Abnormal study	Regions within the cerebral cortex and deep gray nuclei with decreased metabolic activity compared to cerebellum (with the exception of Parkinson plus syndromes which lead to cerebellar hypometabolism)	Uptake in the cerebral white matter with blurring of the corticomedullary junction, with various named signs (tree in summer, kissing hemispheres, etc.)	Increased contiguous neocortical activity, generally involving greater than one area

PET Positron emission tomography, MBq Megabecquerel, mCi Millicurie, mSv Millisievert

Table 2 Synopsis of imaging features of common neurodegenerative disorders

	Typical AD	DLB	VaD	FTD
sMRI	Mesial temporal lobe atrophy	Frontotemporal atrophy	Two or more large territory, three or greater lacunar infarcts, or strategically placed infarcts. Involvement of cerebral hemisphere by greater than 25% WMHs	bv—Ventromedial prefrontal and insular cortical atrophy svPPA—left inferior temporal lobe including the insular gyrus nPPA—posterior frontal, temporal, and parietal lobes
SW/T2*		Swallow tail sign	Microhemorrhages can be present	
MRS	Decreased NAA/myoinositol in the PCC			
DTI	Decreased FA and increased MD in mesial temporal lobe, PCC, SLF	Decreased FA parieto-occipital lobes, PCC, striatum	Reduced FA and increased MD in the centrum semiovale and anterior periventricular white matter	Reduced FA in the UF, genu of the CC, and left ACC
rsfMRI	Hypoconnectivity of DMN	Hypoconnectivity of DMN and visual networks	Hypoconnectivity of DMN	Hypoconnectivity of salience network and disruption of frontoinsular and executive connections
ASL	Hypoperfusion involving the temporo-parietal lobes			Hypoperfusion of the frontal lobes and anterior cingulate cortex
FDG-PET	Temporoparietal hypometabolism	Temporoparietal and occipital hypometabolism Cingulate island sign Occipital tunnel sign	Hypometabolism of the anterior cingulate cortex, deep gray nuclei, primary cortices, and middle temporal gyrus	bv—hypometabolism of ventromedial frontal lobe and anterior temporal lobes svPPA—hypometabolism of left or bilateral temporal poles, middle and inferior temporal gyri, and insula nPPA—hypometabolism of the inferior temporal gyrus, anterior cingulate cortex, and insula with sparing of the amygdala and hippocampi
Amyloid PET	Often diffuse cortical uptake	Majority demonstrate uptake, primarily temporoparietal with more involvement of the occipital lobes compared to AD	At least 25% demonstrate uptake	Generally lack of uptake
Tau PET	Uptake within the temporoparietal neocortical areas—in vivo Braak staging	Inferolateral temporal and parietal lobes with less mesial temporal lobe activity compared to AD		Uptake in the inferior and lateral temporal lobes and temporal poles, and anterior cingulate cortex
DAT/Dopamine imaging		Decreased striatal uptake	Striatal infarcts can lead to decreased uptake	

sMRI structural magnetic resonance imaging, MRS Magnetic resonance spectroscopy, DTI Diffusion tensor imaging, rsfMRI resting-state functional magnetic resonance imaging, ASL Arterial spin labeling, FDG Fluorodeoxyglucose, PET Positron emission tomography, DAT Dopamine transporter, AD Alzheimer's disease, NAA N-acetylaspartate, FA Fractional anisotropy, MD Mean diffusivity, DMN Default mode network, PCC Posterior cingulate cortex, SLF Superior longitudinal fasciculus, DLB Dementia with Lewy bodies, VaD Vascular dementia, WMH White matter hyperintensity, FTD Frontotemporal dementia, bv behavioral variant, PPA Primary progressive aphasia, sv semantic variant, nf nonfluent, UF Uncinate fasciculus

Table 3 Synopsis of imaging features of parkinsonian syndromes

	CBD	PSP	MSA
sMRI	Asymmetric atrophy of the posterior frontal and parietal lobes and cerebral peduncle contralateral to symptoms	“Mickey mouse” and “hummingbird” signs secondary to brainstem atrophy	MSA-p—lateral rim of T2/PD hyperintensity adjacent to putamen (1.5 T) MSA-c—Hot cross bun sign, brainstem and cerebellar atrophy and T2 hyperintensity
SW/T2*			
MRS			
DTI	Reduced FA in the pre- and post-central gyri, cingulum, and SMA	Reduced FA in the posterior frontal lobes and cerebellar peduncles	Reduced FA in the superior, middle, and inferior cerebellar peduncles and in the corona radiata and commissural fibers
rsfMRI	Hypoconnectivity of the lateral visual and auditory networks and hyperconnectivity of the salience and executive control networks	Hypoconnectivity of the lateral visual, auditory, cerebellar, and insular networks	Hypoconnectivity of the DMN, sensorimotor network, visual associated cortices, and cerebellum
ASL			
FDG-PET	Hypometabolism involving the primary cortices and additionally basal ganglia contralateral to the affected side	Hypometabolism involving the brainstem and midline frontal cortex	Hypometabolism involving the bilateral putamina and cerebellar hemispheres
Amyloid PET	May show uptake in CBS (not pure CBD) secondary to underlying amyloid-related NDD		
Tau PET	Uptake of 18-F-PI-2620 in frontoparietal cortices and basal ganglia structures contralateral to affected side	Uptake of 18-F-PI-2620 in the basal ganglia and brainstem structures	
DAT/Dopamine imaging	Asymmetric decreased striatal uptake caudate relatively more impacted than putamen	Decreased striatal uptake	Reduced uptake within the putamina

sMRI structural magnetic resonance imaging, MRS Magnetic resonance spectroscopy, DTI Diffusion tensor imaging, rsfMRI resting-state functional magnetic resonance imaging, ASL Arterial spin labeling, FDG Fluorodeoxyglucose, PET Positron emission tomography, DAT Dopamine transporter, MSA-p MSA-p Multisystem atrophy, Parkinsonian type, MSA-c MSA-c Multisystem atrophy cerebellar type, DMN Default mode network, FA Fractional anisotropy, PSP Progressive supranuclear palsy, CBS Corticobasal degeneration, SMA Supplementary motor area, CBD Corticobasal syndrome, MDD Neurodegenerative disease

Table 4 Synopsis of imaging features of miscellaneous neurodegenerative disorders

	Psd	CJD	HD	ALS	CTE	CAA
sMRI		Cortical ribboning and basal ganglia and thalamic (hockey stick) hyperintensity of T2 or DWI	Atrophy of striatum with ex vacuo dilated "box-shaped" frontal horns of the lateral ventricles	T2 hyperintensity of CSTs and perirolandic regions	Increased preponderance of cavum septum pellucidum with generalized cerebral atrophy	Inflammatory type: lobar vasogenic edema with leptomeningeal enhancement Amyloidoma—solitary enhancing mass with surrounding edema Lobar and subcortical microhemorrhages and superficial siderosis
SW/T2*				Increased iron deposition in motor cortex		
MRS		Decreased NAA of affected regions		Decreased NAA in the CSTs		
DTI			Increased FA and MD in the basal ganglia	Reduced FA in the CSTs	Reduced FA in superior and inferior longitudinal fasciculus, corona radiate, cerebral peduncle, uncinate fasciculus, anterior thalamic radiations, and striatum	
rsfMRI				Hypoconnectivity of the motor network		
ASL						
FDG-PET	Generally normal	Asymmetric hypometabolism in the frontal and parietal cortices with or without decreased activity in the basal ganglia	Hypometabolism in the striatum and frontal and temporal lobes	Hypometabolism of the motor/perirolandic and frontal cortices and occipital lobes	Hypometabolism in the frontotemporal lobes	Hypometabolism in pattern similar to AD with increasing occipital to global or PCC ratio
Amyloid PET	Generally normal	No significant uptake			Variable uptake	Uptake in pattern similar to AD with increasing occipital to global or PCC ratio
Tau PET	Generally normal	Off-target binding of certain tracers felt to be related to astrocytosis		[11C]PBB3 uptake in the CSTs	Uptake in the frontotemporal lobes including the medial temporal lobes	Neocortical uptake correlates with worsening cognition
DAT/Dopamine imaging			Decreased striatal dopamine receptor binding			

sMRI structural magnetic resonance imaging, MRS Magnetic resonance spectroscopy, DTI Diffusion tensor imaging, rsfMRI Resting-state functional magnetic resonance imaging, ASL Arterial spin labeling, FDG Fluorodeoxyglucose, PET Positron emission tomography, DAT Dopamine transporter, CAA Cerebral amyloid angiopathy, AD Alzheimer's disease, PCC Posterior cingulate cortex, CTE Chronic traumatic encephalopathy, FA Fractional anisotropy, ALS Amyotrophic lateral sclerosis, CSTs Corticospinal tracts, NAA N-acetylaspartate, HD Huntington's disease, CJD Creutzfeldt–Jakob disease, DWI Diffusion-weighted imaging, PsD Pseudodementia

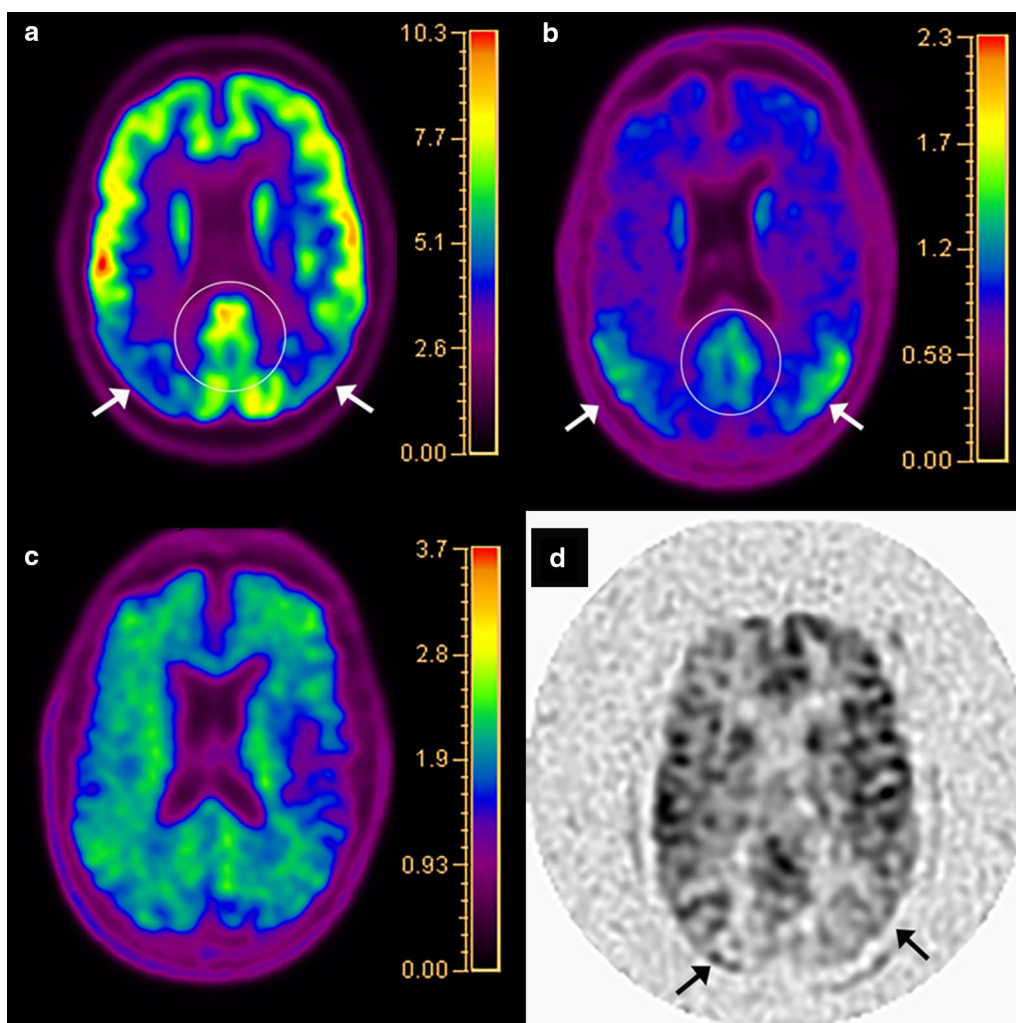


Fig. 3 A 73-year-old man with AD, Mini Mental State Examination (MMSE) 23/30. Fluorodeoxyglucose PET/CT **(a)** demonstrates hypometabolism involving the bilateral parietal lobes (arrows) and precuneus and PCC (oval). Flortaucipir PET/CT **(b)** shows tau retention in the bilateral parietal lobes (arrows) and precuneus and PCC (oval), mirroring the regions of hypometabolism. Florbetapir PET/CT **(c)** demonstrates diffuse cortical uptake with “kissing hemispheres.” Arterial spin labeling **(d)** demonstrates hypoperfusion to the bilateral parietal lobes (arrows), similar to the FDG-PET/CT

Lilly, USA), and flutemetamol (Vizamyl GE Healthcare, USA) are commonly used F-18 labeled Aβ selective radiotracers, with third-generation tracers in development and preclinical trials. These tracers have also shown robust ability to distinguish AD from controls with pooled analysis demonstrating a sensitivity and specificity of 90% and 87% for florbetapir and 89% and 88% for florbetaben [51]. Amyloid imaging has shown added value to FDG-PET and clinical evaluation [52]. Qualitative interpretation of amyloid imaging is either considered positive (moderate to frequent amyloid plaque) or negative (no to sparse amyloid plaque) based on abnormal gray matter uptake on grayscale imaging in one or two regions for florbetaben and florbetapir respectively, or one region on rainbow color scale for flutemetamol

[53–55]. Normal studies exhibit physiologic uptake within the white matter with the absence of uptake in the gray matter creating many named imaging signs, including the “diamond” of the white matter tracts of the orbitofrontal gyri, “cartoon hand” and “tree in winter” in the white matter of the frontal lobes, “double convex lens” involving the frontal and parietal parasagittal region, and the “temporo-occipital ridge” (Fig. 5) [56]. Abnormal regions demonstrate radiotracer activity within the gray matter, leading to blurring of the gray matter-white matter junction with most common sites including the precuneus, PCC, and lateral temporal and parietal lobes. The activity within the gray matter leads to the appearance of “kissing hemispheres” along the interhemispheric fissure, “tree in summer” when viewed in the coronal plane, and

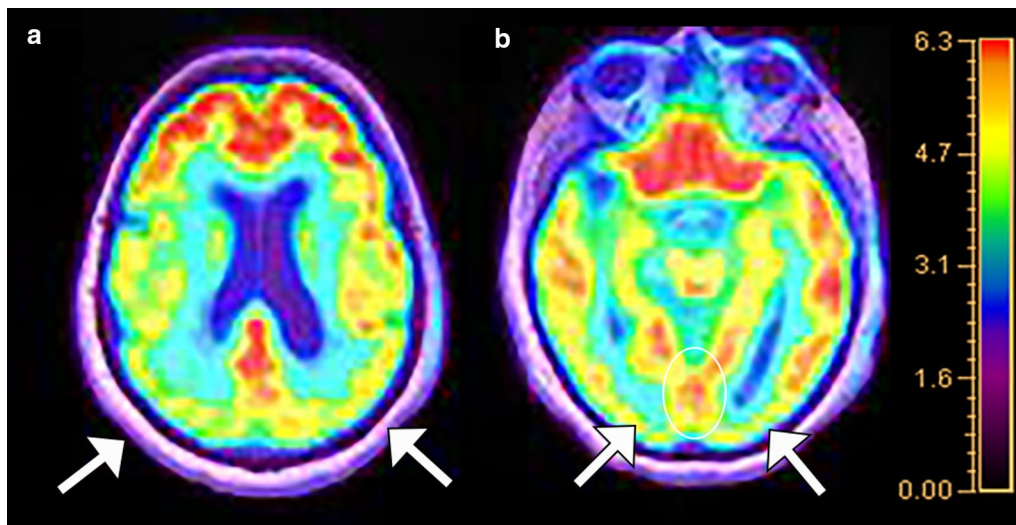


Fig. 4 A 76-year-old woman with history of memory loss. Fluorodeoxyglucose PET/MRI (**a**) demonstrates hypometabolism of the parietal lobes (arrows), precuneus, and PCC as well as the visual association centers in the lateral occipital lobes (arrows in **b**). Metabolic activity is preserved in the medial occipital lobes (“occipital tunnel sign,” white oval in **b**). Pattern of hypometabolism is most suggestive of posterior cortical atrophy

a “temporal plain” as opposed to a “temporo-occipital ridge” (Fig. 5) [9, 12, 56]. Even small amounts of amyloid plaques may be predictive of eventual development of AD [57]. Positron emission tomography amyloid imaging has shown similar diagnostic accuracy to cerebrospinal fluid (CSF) analysis, with the obvious advantage of negating an invasive procedure [58]. Amyloid imaging may also be used to follow patients on monoclonal antibody therapy to demonstrate clearance of A β plaques (Fig. 6).

Semiquantitative analysis can also be performed for PET amyloid studies by calculating a standardized uptake value ratio (SUVr). This is achieved by first selecting a region of interest to determine baseline, most often the cerebellar gray matter as this rarely accumulates amyloid, and comparing the ratio of uptake in this region to specified regions of interest (ROIs) [59]. If the region demonstrates a SUVr above a predetermined threshold, it is considered positive for moderate to frequent amyloid plaque [60]. Currently there is debate in the literature about whether qualitative or semiquantitative interpretation of amyloid imaging is more efficacious [61, 62]. Additionally, as with FDG-PET, ss-SPM can be

undertaken to increase diagnostic confidence. While the literature at the time is sparse, coupling these techniques with amyloid PET imaging has shown promising results in terms of diagnostic accuracy, with sensitivity and specificity near or surpassing 90% [63]. Dynamic imaging can also be performed immediately following the bolus to estimate cerebral blood flow, with a report suggesting decreased early time frame amyloid activity correlating with tau retention [64].

Tau selective radiotracers can also be utilized for disease-specific imaging of AD. Currently, the most widely used tau selective radiotracer is older-generation F-18 flortaucipir (Tauvid; Avid Radiopharmaceuticals, previously known as AV 1451 and T807) [65]. The limitation of this older-generation tau radiotracer is substantial off-target binding, with one study reporting 64% of the signal in amyloid negative healthy controls was due to off-target binding primarily from the basal ganglia structures and choroid plexuses [66]. Off-target binding can also occur in the muscles and secondary to monoamine oxidase (MAO) enzymatic activity in astrocytes in non-specified neuroinflammation. Newer-generation tau radiotracers

(See figure on next page.)

Fig. 5 Named signs of normal and abnormal patterns of amyloid activity on florbetapir PET/CT. Normal activity in the white matter of the frontal lobes leads to the “tree-in-winter sign” on coronal images, abnormal activity in the gray matter leads to the appearance of leaves known as the “tree-in-summer sign” (**a, b**). Absence of gray matter activity in the medial orbitofrontal lobes creates a diamond pattern of the white matter activity which is lost in abnormal studies (**c, d**). A similar phenomenon is seen at the cerebral convexities where the superior white matter tracts create the “double convex lens sign” (**e**) which is lost with abnormal gray matter activity morphing to the “kissing hemispheres sign” (**f**). Lastly, normal absence of gray matter activity in the temporal and occipital lobes creates a mountainous façade referred to as the “temporo-occipital ridge” (**g**), whereas abnormal gray matter activity leads to a more flat profile termed the “temporo-occipital plain” (**h**)

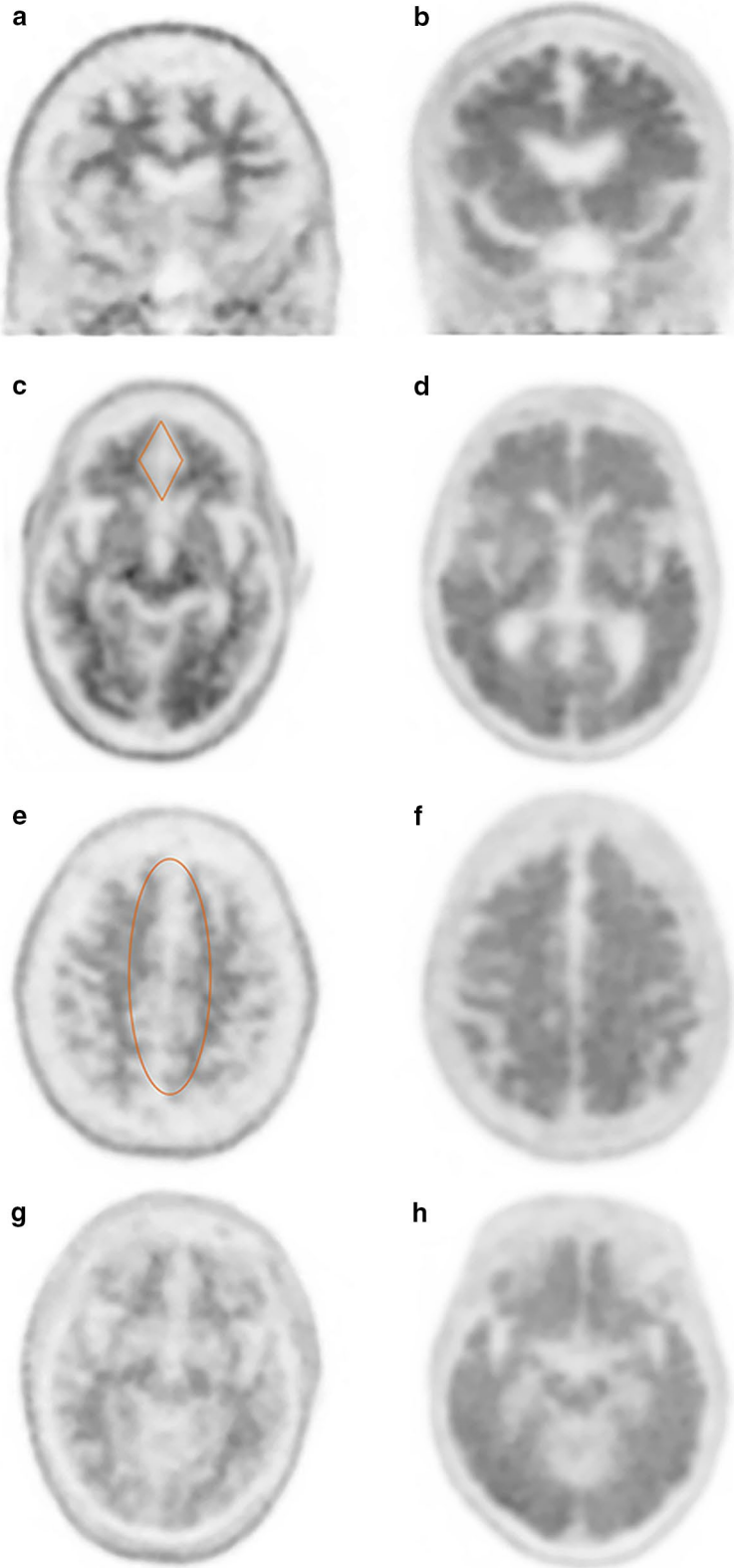


Fig. 5 (See legend on previous page.)

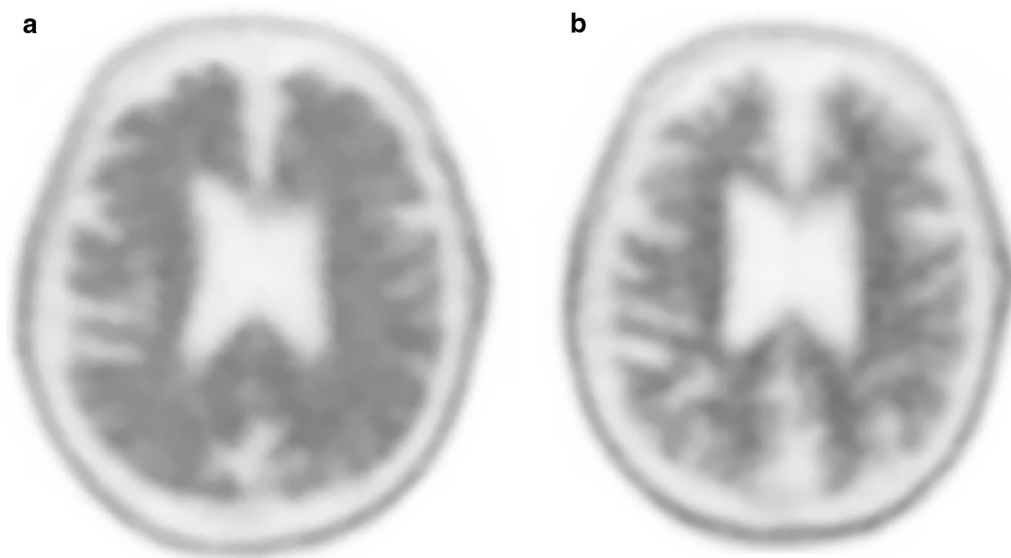


Fig. 6 A 83-year-old male with typical AD on anti-A β monoclonal antibody clinical trial drug. Pre-treatment florbetapir PET/CT demonstrates substantial cortical amyloid burden with kissing hemispheres in midline (a). Following treatment there is significant reduction in amyloid uptake with visualization of corticomedullary differentiation reminiscent of a normal scan (b)

including F-18RO-948 (previously RO69558948), F-18-MK6240, F-18-PI2620, and F-18-GTP1 are under investigation [67–71]. Carbon-11 labeled tau radiotracers are also being studied, although as with PiB, C-11 labeled radiotracers will inherently be limited by short half-life [68, 72]. Fluorine-18-RO-948, F-18-MK6240, and F-18-GTP1 have been shown to have greater affinity for tau than F-18 flortaucipir [70, 72, 73]. In contrast to amyloid imaging, tau imaging allows for better visualization of the topography of the pathologic changes of AD. The earliest regions of radiotracer uptake are in the mesial temporal lobes including the entorhinal cortices and hippocampi, progressing to the middle and inferior temporal lobes, parietal lobes including the angular and supramarginal gyrus, cingulate cortex, and dorsolateral frontal lobes, with groups showing promise of in vivo Braak staging using tau PET imaging [74, 75]. A recent study demonstrated a sensitivity of 92.3% to 100.0% and specificity ranging from 52.0 to 92.0% for identifying Braak stage V or VI disease at postmortem evaluation for F-18 flortaucipir (Fig. 7) [76]. Tau imaging may also differentiate between AD subtypes better than amyloid and closely mirrors cortical gray matter atrophy and FDG-PET hypometabolism [77–79]. As with amyloid radiotracers SUVr values can be calculated, again generally using the cerebellum for the reference value [80].

Lastly, ongoing research is being performed to utilize molecular imaging for the evaluation of neuroinflammation and synaptic density in AD with a variety of C-11 and F-18 labeled radiotracers, none of which are currently widely used clinically. An 18 kDa translocator

protein is the typical target for microglial activation with the most widely used tracer 11C-PK11195 [81]. Astrocytosis in AD is imaged by targeting MAO-B with 11C-deuterium-l-deprenyl (11C-DED) [82]. Studies have reported increased and no significant difference in microglial activation in AD patients when compared to controls [83–86]. Temporal changes in astrocytosis have been reported, with increased radiotracer activity in prodromal AD followed by a gradual decline in activity as the disease progresses which correlates with hypometabolism [87–89]. Uptake of radiotracers 11C-UCB-J and 18F-UCB-H, which bind to the synaptic glycoprotein 2, have been shown to be reduced in the hippocampi of patients with AD [90–93].

Dementia with Lewy bodies

Dementia with Lewy bodies (DLB) is considered the second or third most common dementia, accounting for approximately 5% of all dementia cases in incidence studies, and up to approximately 20% of all dementia cases in prevalence studies [94]. Clinically DLB is defined by fluctuating cognition, visual hallucinations, rapid eye motion sleep behavior disorder, and parkinsonism [95]. Pathologically DLB is defined by loss of dopaminergic neurons in the substantia nigra with reduced striatal dopaminergic activity and neuronal inclusions of alpha-synuclein-positive Lewy bodies in the cerebral cortex, substantia nigra, and brainstem. These findings are indistinguishable from Parkinson's disease (PD); however, the involvement of the cortex may be more pronounced in DLB and neuronal

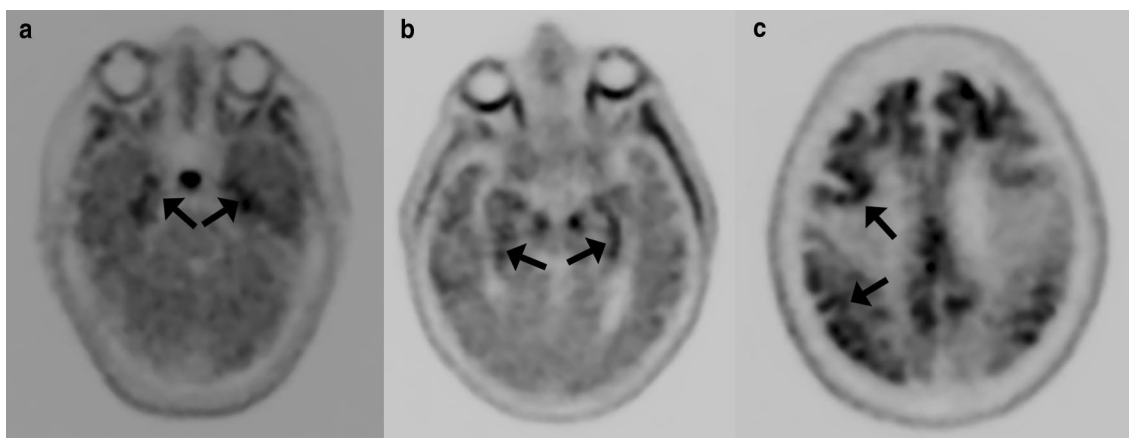


Fig. 7 In vivo Braak staging on flortaucipir PET/CT. Activity confined to the entorhinal cortices and hippocampi falls into the Braak I-II stages (arrows in **a**), further progression in the temporal lobes and limbic cortices classifies stages III-IV (parahippocampal gyri; arrows in **b**), and neocortical activity defines stages V-VI (arrows in **c**)

loss in the substantia nigra more prominent in PD [96]. In addition, there are often concomitant A β plaques and 3R/4R NFTs and over-expression of the APOE*E4 genotype, overlapping with the pathologic features of AD [97, 98].

As with AD, structural MRI plays a role in the assessment of DLB. T1 volumetric analysis of patients with DLB demonstrates atrophy of the frontal and temporal lobes and insular cortices with less pronounced involvement of the medial temporal lobe when compared to AD, hypothesized to be related to comparatively reduced NFT formation [99, 100]. Sparse partial least squares classification of cortical thickness based on T1-weighted imaging demonstrated good discrimination of DLB from AD with a sensitivity of 78% and specificity of 75% [101]. Atrophy of the midbrain, hypothalamus, and substantia innominate have also been shown to be useful in discriminating DLB from AD [102].

Advanced MRI techniques have also been reported to be of value in the diagnosis of DLB. Studies have shown decreased FA involving the cortical and subcortical regions including the parieto-occipital lobes, PCC, precuneus, inferior longitudinal fasciculus, caudate, putamen, and pons [103–106]. Abnormalities in FA in the parietal and occipital regions in DLB have been shown to not significantly change over time when compared to controls, corroborating the theory DLB is primarily associated with synaptic dysfunction rather than neuronal loss [107]. Absence of the “swallow tail sign,” hypointensity within nigrosome-1 on susceptibility-weighted imaging, has been reported to have a sensitivity of 63–93% and a specificity of 79–87% in discrimination DLB from other forms of dementia (Fig. 8) [108, 109]. A similar finding was demonstrated with postmortem MTI with

lower signal in the substantia nigra pars compacta in patients with DLB and PD, potentially secondary to neuromelanin loss [110]. Regions of decreased contrast-to-noise ratio in the LC on MTI have been shown to relate to symptoms in PD [111]. Similar to AD, rsfMRI exhibits decreased connectivity in the default mode and executive networks and additionally the visual networks including the medial occipital network [112, 113].

Molecular imaging also plays a crucial role in the diagnosis and potentially response to therapy of DLB. Dopamine transporter (DAT) imaging has been a target for DLB, specifically the imaging of the density of the presynaptic striatal neurons to assess for degeneration in presynaptic parkinsonian syndromes. Single-photon emission computed tomography (SPECT) imaging with iodine-123 N- ω -fluoropropyl-2 β -carbomethoxy-3 β -[4-iodophenyl] nortropine (I-123-FP-CIT, DaTSCANTM, GE Healthcare), a cocaine analogue with high affinity for the dopamine and serotonin transporters allowing for in vivo evaluation of presynaptic striatal neuronal degeneration, was initially used clinically for discriminating PD from essential tremor on the basis of excellent reported specificity [114]. As PD and DLB share the same pathologic basis, I-123-FP-CIT has shown similar value in the diagnosis of DLB, with a diagnostic accuracy around 90% in discriminating from other dementia syndromes; however, DAT imaging is not reliable for discriminating DLB from PD-related MCI or dementia [115, 116]. Single-photon emission computed tomography imaging with I-123-Metaiodobenzylguanidine to assess for cardiac postganglionic sympathetic denervation observed in DLB is reported to have similar sensitivity and specificity to I-123-FP-CIT SPECT,

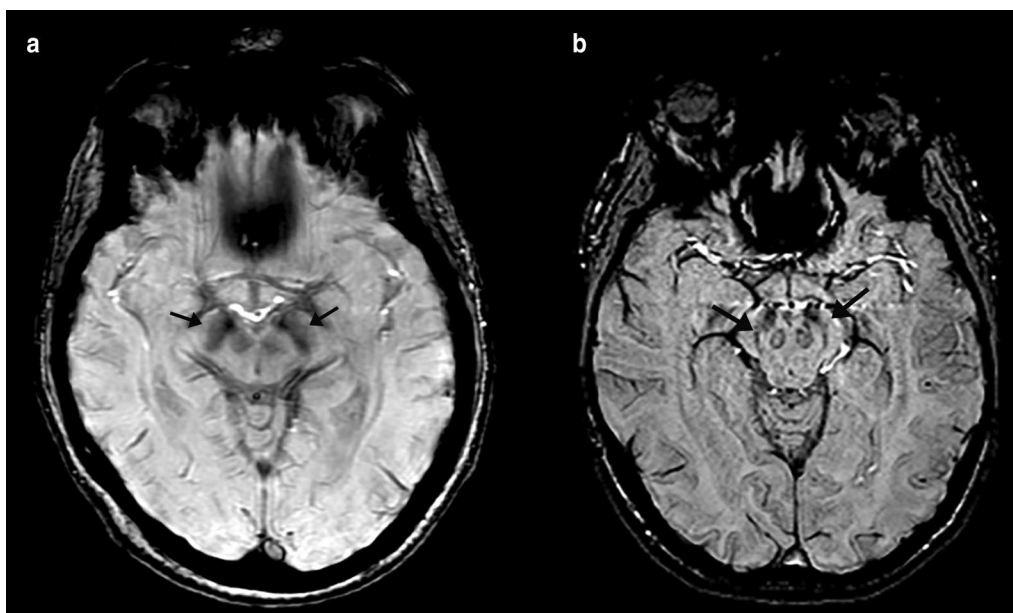


Fig. 8 A 82-year-old female with history of rigidity, bradykinesia, hallucinations, and dementia. Axial susceptibility-weighted imaging demonstrates loss of the normal hyperintense signal in nigrosome-1 (arrows), the so-called loss of “swallow tail sign” (a). The normal hyperintense signal in nigrosome-1 is shown in (b) (arrows)

although pre-existing cardiac disease and diabetes mellitus can lead to false positives [117, 118].

Positron emission tomography imaging can also be performed to evaluate for DLB. Decreased metabolic activity in the occipital, temporoparietal, and pre-frontal cortices with relative sparing of the pre- and post-central gyri and medial temporal lobes has been reported in DLB [119]. Additionally, there is relatively preserved FDG uptake within the PCC, with surrounding hypometabolic activity in the cuneus and precuneus and parietal lobes, creating the so-called cingulate island sign, reported to have excellent specificity of up to 100% in differentiating AD from DLB when present (Fig. 9) [120]. The “occipital tunnel sign” is also seen in DLB, which is characterized by hypometabolism in the visual association cortex of the lateral occipital lobes and preserved metabolism in the medial occipital lobes [38]. Other studies have demonstrated less promising results for FDG-PET in differentiating DLB from AD, indicating the value of a multimodality assessment [115].

As DLB can pathologically demonstrate A β plaques and NFTs, both amyloid and tau tracers can be of value in the imaging of DLB. The majority of DLB patients show amyloid uptake, with a similar pattern to AD involving the dorsolateral frontal lobes, parietal lobes including the precuneus, and temporal lobes, with greater amyloid

deposition in the occipital lobes in DLB [121, 122]. Multiple groups have reported the degree of amyloid burden may be related to cognitive decline in DLB and helpful in differentiating DLB from PD-related dementia (PDD) [122–124]. Combined amyloid and dopamine terminal PET imaging was reported to have high accuracy in diagnosing dementia subtype when compared to pathologic examination [125]. Tau PET imaging is less well studied in DLB, with typical areas of increased uptake involving the inferolateral temporal lobes, parietal lobes including the precuneus, and occipital lobes, with decreased degree of uptake and involvement of the medial temporal lobes when compared to AD, with DLB again showing greater abnormality compared to PDD [126, 127]. Attempts at developing a radiotracer to target alpha-synuclein, the pathologic hallmark of DLB, have not been successful at the current time [128–130].

Vascular dementia

Vascular dementia (VaD) is considered the second or third most common dementia, varying with DLB by source [131]. There are multiple subtypes of vascular dementias, attributed to small vessel and large vessel etiologies as well as acquired and inherited conditions, such as cerebral autosomal dominant arteriopathy with subcortical infarcts and leukoencephalopathy (CADASIL). Clinical presentation is heterogeneous, with the most

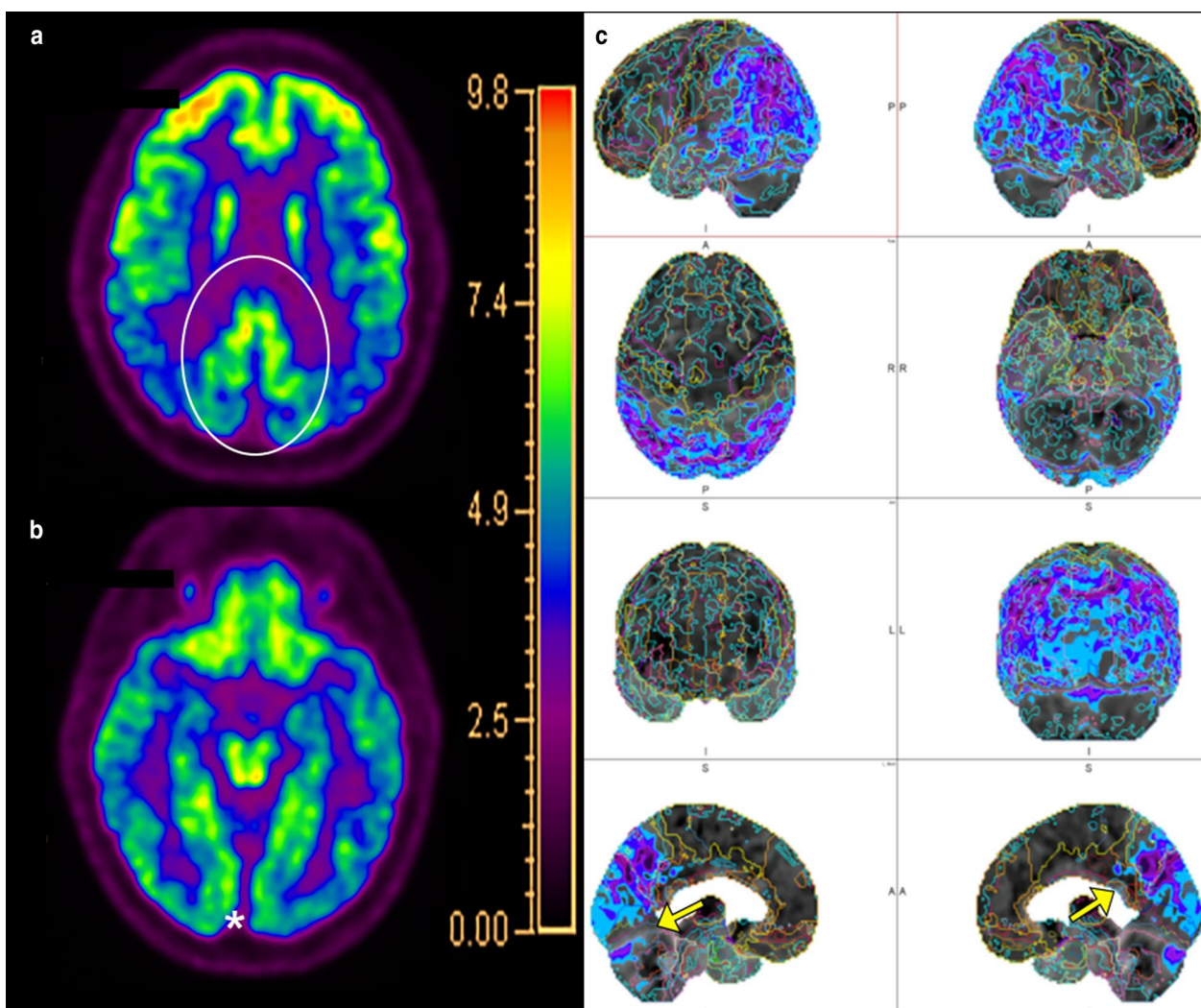


Fig. 9 A 73-year-old man with memory loss and visuospatial processing deficits. Fluorodeoxyglucose PET/CT demonstrates hypometabolism in the bilateral parietal lobes including the bilateral precuneus with preserved metabolism of the PCC (cingulate island sign, oval in **a**). Also present is hypometabolism of the bilateral lateral occipital lobes with preserved medial occipital lobe activity (occipital tunnel sign, asterisk in **b**). Single-subject statistical parametric mapping (**c**) demonstrates parietal-occipital hypometabolism reiterating the occipital tunnel (arrow bottom left panel) and posterior cingulate island (arrow bottom right panel), with areas of blue progressing to purple representing further negative deviation from the mean uptake values of controls

prominent feature decline in frontal lobe tasks including executive function and attention with verbal memory less impacted [132]. VaD also has a strong correlation with neuropsychiatric symptoms including depression [133].

Structural MRI has long held a central role in the evaluation of VaD. Two or more large territory, three or greater lacunar infarcts, or strategically placed infarcts have been considered sufficient imaging evidence for VaD by various guidelines [134, 135]. Involvement of greater than 25% of a cerebral hemisphere with white matter abnormalities/hyperintensities (WMHs) can be suggestive of subcortical VaD, although there is inter-observer variation in making the diagnosis [136, 137].

Dilated Virchow-Robins spaces have also been correlated with the degree of severity of subcortical VaD [138]. Diffusion tensor imaging may predict the structural changes in VaD even prior to development of WMHs and better predicts decline in cognition with reduced FA and increased MD reported in the centrum semiovale and anterior periventricular white matter [139, 140]. Reduced FA and increased MD in the inferior fronto-occipital fascicles, forceps minor, genu, and splenium of the corpus callosum, and the superior longitudinal fasciculus have shown value in discriminating VaD from AD [141]. Early studies of rsfMRI demonstrate dysfunction involving the DMN [142].

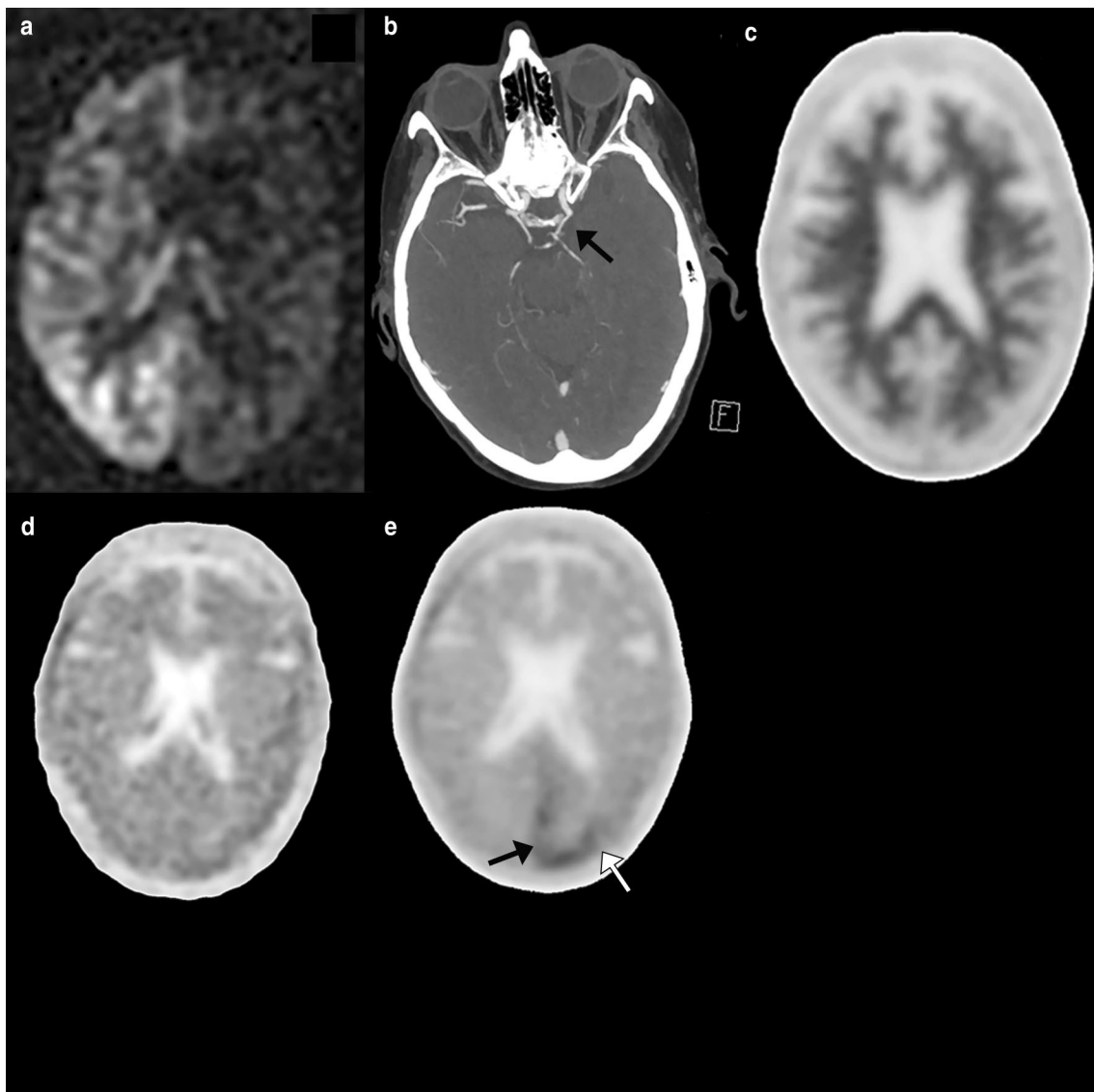


Fig. 10 A 76-year-old female with symptomatic left carotid stenosis (70% by North American Symptomatic Carotid Endarterectomy Trial criteria) who presented with right homonymous hemianopia compatible with a left posterior cerebral artery stroke. Arterial spin labeling demonstrates hypoperfusion throughout the left cerebral hemisphere (**a**) and CTA demonstrates a fetal left posterior cerebral artery supplied by the left internal carotid artery (**b**). Florbetaben PET/CT demonstrates no to sparse amyloid plaque (**c**). Flortaucipir PET/CT prior to the event demonstrates no areas of cortical tau retention (**d**). Flortaucipir PET/CT following the event (**e**) demonstrates focal tau retention in the left posterior cerebral artery territory (arrows), likely as a response to cerebral ischemia

Molecular imaging has a developing role in the evaluation of VaD. Hypometabolism in VaD is pronounced in structures spared in early AD including the anterior cingulate cortex, deep gray nuclei, primary cortices, and middle temporal gyrus, with Kerrouche et al. reporting 100% accuracy in separating VaD from AD [143, 144]. Amyloid imaging is less helpful in discriminating between VaD and AD, with at least a quarter of VaD patients demonstrating amyloid uptake and those that are PiB positive have similar distribution to AD [145–147]. Positive

amyloid imaging, however, may predict worse cognitive function in VaD [146, 148]. While it is known tau deposition occurs following cerebral ischemia (Fig. 10), reports of tau tracers in the evaluation of VaD are lacking [149].

Frontotemporal dementia

Frontotemporal dementia (FTD) or frontotemporal lobar degeneration (FTLD) is the second most common NDD in patients under 65 years of age, only behind AD [150]. The estimated prevalence is approximately 1–5 in

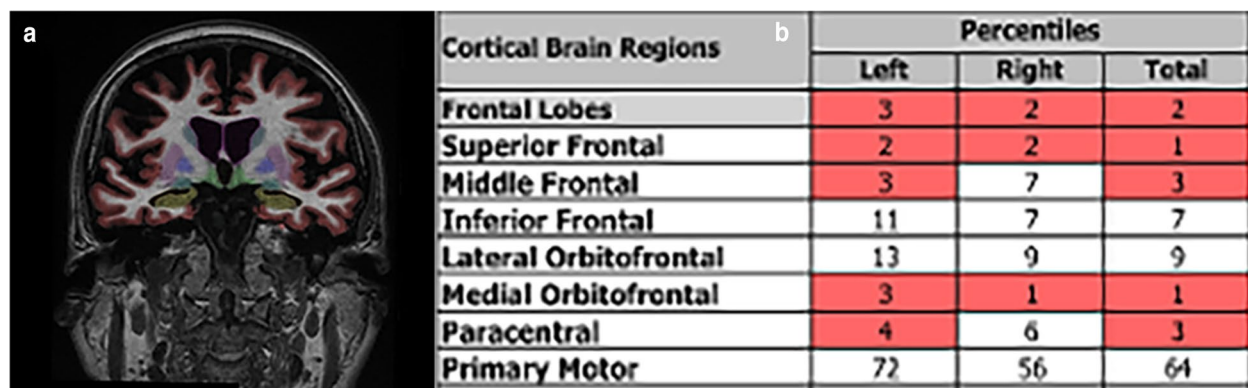


Fig. 11 A 69-year-old female with odd behaviors including riding a children's tricycle and impulsivity. Coronal volumetric T1-weighted images with proprietary automated segmentation software demonstrate volume loss in the frontal and temporal lobes (a). Volumetric quantitation identifies multiple regions in the frontal lobes in less than the fifth percentile of volume for age, including the medial orbital frontal lobes, typical of bvFTD (b)

100,000 people [151, 152]. There is an equal predilection of the disease between men and women, most commonly diagnosed between the ages of 45 and 65; however, patients can be diagnosed as early as the second to third decade [150]. The most common subtype is the behavioral variant (bvFTD), characterized by social disinhibition, obsessive behaviors, and hyperorality, as well as the aptly named semantic (svPPA) and nonfluent/agrammatic primary progressive aphasia (nfPPA). Three distinct pathologic subtypes are described; first Pick reported argyrophilic cytoplasmic inclusions (of predominantly 3R tau) within cortical neurons leading to ballooning of the cells and eventually gliosis, later TAR DNA-binding protein 43 (TDP-43) and fused-in-sarcoma (FUS) pathologic variants were described [153, 154]. Heritable forms make up at least 10% of cases, including those with microtubule-associated protein tau (MAPT), Chromosome 9 Open Reading Frame 72 (C9ORF72), and Progranulin mutations [150, 155].

As with the other neurodegenerative syndromes, volumetric T1-weighted imaging to assess for patterns of atrophy is commonly applied in FTD. Behavioral variant FTD tends to demonstrate marked atrophy involving the ventromedial prefrontal and insular cortices and anterior temporal lobes (Fig. 11), svPPA in the left inferior temporal lobe including the insular gyrus, and nfPPA in the posterior frontal, temporal, and parietal lobes [156]. Resting-state functional MRI has most consistently reported disruption of the salience network and fronto-insular and executive connections [157–159]. One study showed patients with FTD exhibit hypoperfusion on ASL in the frontal lobes and anterior cingulate cortex, with the hypoperfusion within the anterior cingulate cortex helping to differentiate FTD from AD [160]. Decreased stiffness by MRE in the temporal lobes has been reported [30].

Molecular imaging plays a crucial and ever-growing role in the evaluation of FTD. Unsurprisingly, hypometabolism corresponding to regions of atrophy in the frontal lobes, including the ventromedial region and anterior temporal lobes has been frequently reported in FTD (Fig. 12) [161, 162]. Fluorodeoxyglucose PET is also an important tool in distinguishing the PPA variants with ss-SPM demonstrating hypometabolism in the left or bilateral temporal poles, middle and inferior temporal gyri, and insula in svPPA and a more heterogeneous pattern of decreases in the inferior temporal gyrus, anterior cingulate cortex, and insula with sparing of the amygdala and hippocampi in nfPPA (Fig. 13) [40, 163]. Initial work on tau-labeled tracers in FTD has primarily been in patients harboring the MAPT mutation as they are known to have tau-related pathology; however, TDP-43-related syndromes have also demonstrated uptake with the basal and medial frontal lobes, inferior and lateral temporal lobes and temporal poles, and anterior cingulate cortex with the most involved regions varying by disease subtype [164, 165]. One study demonstrated co-localization between tau binding and microglial activation [166]. Lack of uptake of amyloid labeled radiotracers can differentiate FTD from AD [167]. Table 2 describes the common imaging features of Typical AD, DLB, VaD, and FTD.

Parkinson's disease and parkinsonian syndromes

Parkinsonian disorders are a heterogeneous group of syndromes sharing the clinical features of extrapyramidal symptoms and bradykinesia and common pathology related to alpha-synuclein and tau with degeneration of the nigrostriatal pathway. These conditions afflict at least 1% of the worldwide population greater than 70 years of age [168]. The differences between Parkinson's disease and DLB have been previously discussed in the DLB section. Three of the most relevant parkinsonian syndromes

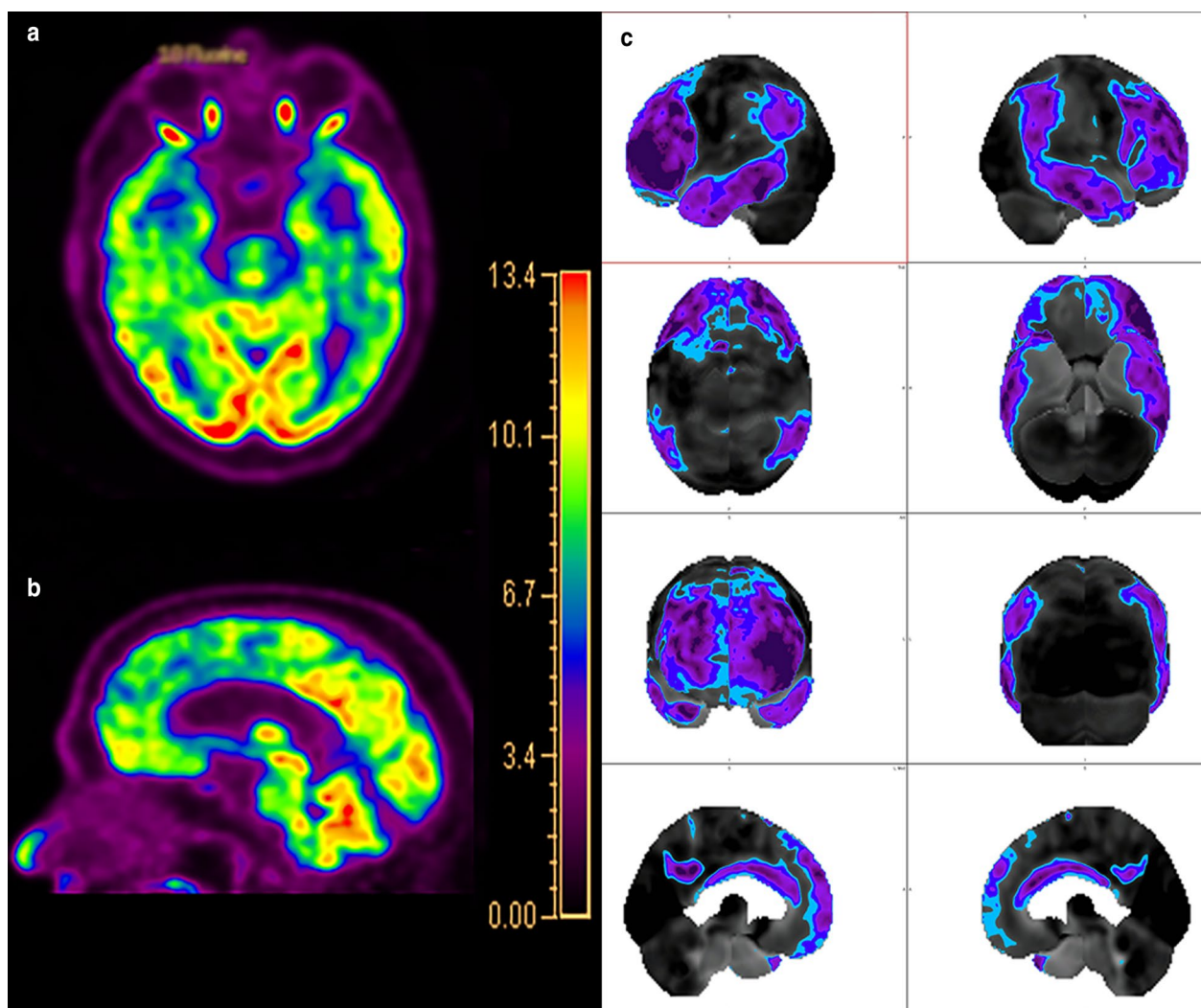


Fig. 12 A 68-year-old man who presented to the memory care clinic with progressive personality changes and behavioral disturbances including violent outbursts and memory loss. Fluorodeoxyglucose PET/CT demonstrates marked frontal (a) and temporal (b) hypometabolism with relatively preserved parietal and occipital lobe activity including relative sparing of the PCC and precuneus. Single-subject statistical parametric mapping (c) from a similar patient demonstrates a similar pattern, with anterior greater than posterior cingulate hypometabolism, a hallmark of FTD, again with areas of blue progressing to purple representing further negative deviation from the mean uptake values of controls

will be reviewed; multisystem atrophy (MSA), progressive supranuclear palsy (PSP), and corticobasal degeneration (CBD).

Multisystem atrophy is a neurodegenerative disorder with multiple subtypes characterized clinically by parkinsonism with varying cerebellar, autonomic, and pyramidal dysfunction sharing common alpha-synucleinopathy pathology [169]. Two main subtypes exist, one with dominant parkinsonian features (MSA-P), and one with dominant cerebellar dysfunction (MSA-C) [170]. On structural 1.5 T MRI, MSA-P has been reported to have a characteristic appearance of a lateral rim of T2/proton density-weighted hyperintensity adjacent to the

putamen and T2 hypointense signal involving the dorsolateral putamen, although the value of this finding has been questioned at higher field strengths (Fig. 14) [171, 172]. The hallmark imaging feature seen in up to 80% of patients with MSA-C is cruciform T2 hyperintense signal within the basis pontis, the so-called hot cross bun sign, although this imaging finding can also be present in spinocerebellar ataxia syndromes (Fig. 15) [173]. Additional structural imaging features of MSA-C include atrophy and T2 hyperintense signal within the pons, medulla, middle cerebellar peduncles, and cerebellar hemispheres [174, 175]. Diffusion tensor imaging exhibits widespread microstructural alterations when compared to controls

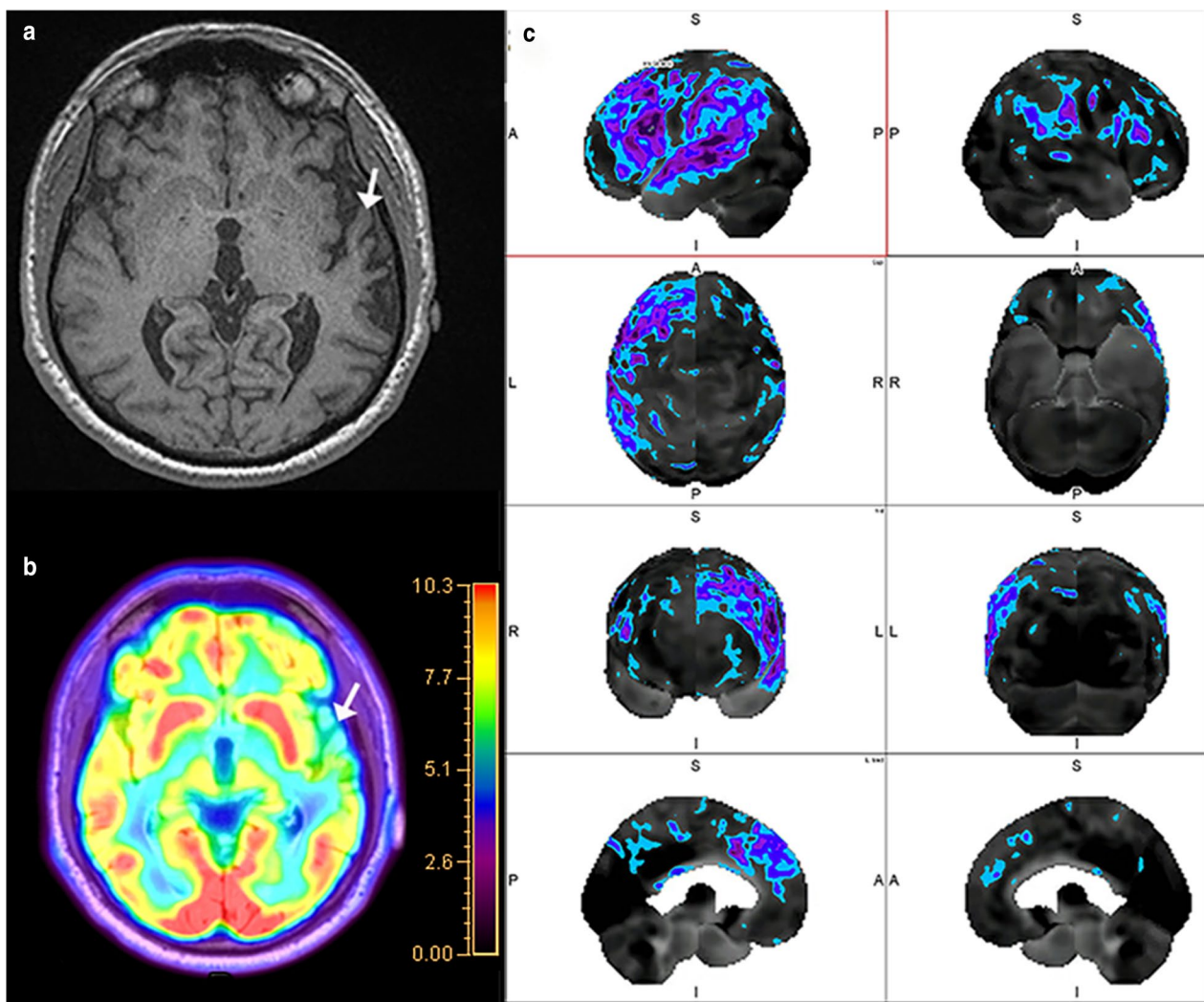


Fig. 13 A 58-year-old man with notable agrammatism, impaired comprehension and repetition of syntactically complex sentences, and spared single word comprehension, Montreal Cognitive Assessment (MoCA) 16/30. T1-weighted volumetric image (a) demonstrates asymmetric atrophy of the left perisylvian and insular cortices (arrow). Fluorodeoxyglucose PET/MRI demonstrates hypometabolism in this region (arrow in b). Single-subject statistical parametric mapping of the FDG-PET/MRI (c) demonstrates the asymmetric left greater than right hypometabolism involving the frontal and temporal operculum and parietal lobes with sparing of the PCC and precuneus (as before, areas of blue progressing to purple represent further negative deviation from the mean uptake values of controls). Combining the clinical and imaging data, a diagnosis of nfPPA was rendered

including increased MD and reduced FA in the superior, middle, and inferior cerebellar peduncles and in the corona radiata and commissural fibers [176]. Patterns of reduced MTR have been shown to help differentiate MSA from PD and PSP [177]. Hypoconnectivity in the DMN, sensorimotor network, visual association cortices, and cerebellum has been reported in MSA-C [178]. Within the same study hypoperfusion of the cerebellum was exhibited on ASL imaging [178]. On FDG-PET MSA is distinguished by hypometabolism involving the

bilateral putamina and cerebellar hemispheres, with the cerebellar hypometabolism reported in both MSA-C and MSA-P, with a sensitivity of 76% and specificity of 98% for the diagnosis by visual interpretation (Fig. 14) [179]. While MSA shows reduced uptake within the putamina on I-123-FP-CIT SPECT scans, this was not shown to correlate with disease severity [180].

Progressive supranuclear palsy is clinically defined by parkinsonism with vertical supranuclear gaze palsy and prominent postural instability with falls within the first

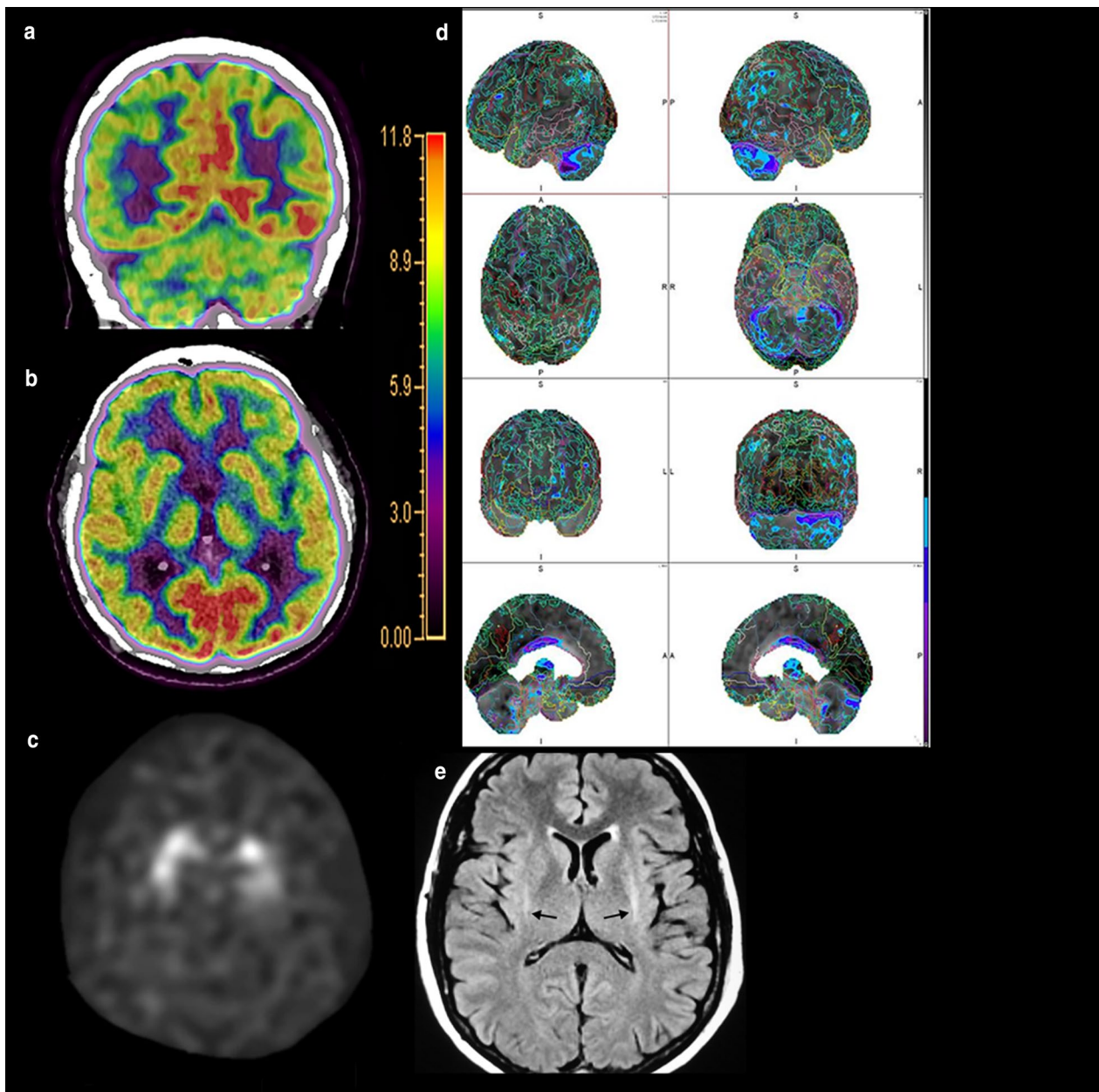


Fig. 14 A 76-year-old man with a history of memory impairment and parkinsonism including gait and proprioceptive dysfunction. Fluorodeoxyglucose PET/CT demonstrates hypometabolism in the right greater than left cerebellar hemispheres (**a**) and bilateral striatum (**b**), best appreciated on ss-SPM (areas of blue and purple representing negative deviation in uptake from controls, **d**). Iodine-123-FP-CIT scan shows left greater than right primarily putaminal presynaptic neuronal degeneration (**c**). Findings are compatible with MSA-P. Axial T2 FLAIR image of a separate patient demonstrates the lateral putaminal rim sign of hyperintensity (arrows in **e**)

year of onset and pathologically by 4R tau isoform NFTs in the basal ganglia, diencephalon, and brainstem [181, 182]. As with MSA, characteristic patterns of brainstem atrophy are present including reduced anterior–posterior dimension of the midbrain and widening of the interpeduncular cistern leading to the “mickey mouse sign” on axial and the “hummingbird sign” on sagittal

images (Fig. 16) [183, 184]. Reduced FA in the posterior frontal lobes and cerebellar peduncles was reported to have a specificity of 91–96% and sensitivity of 85–95% in differentiating PSP from DLB [185]. Hypoconnectivity on rsfMRI has been documented of the lateral visual, auditory, cerebellar, and insular networks [186]. Typical findings of FDG-PET include hypometabolism of the

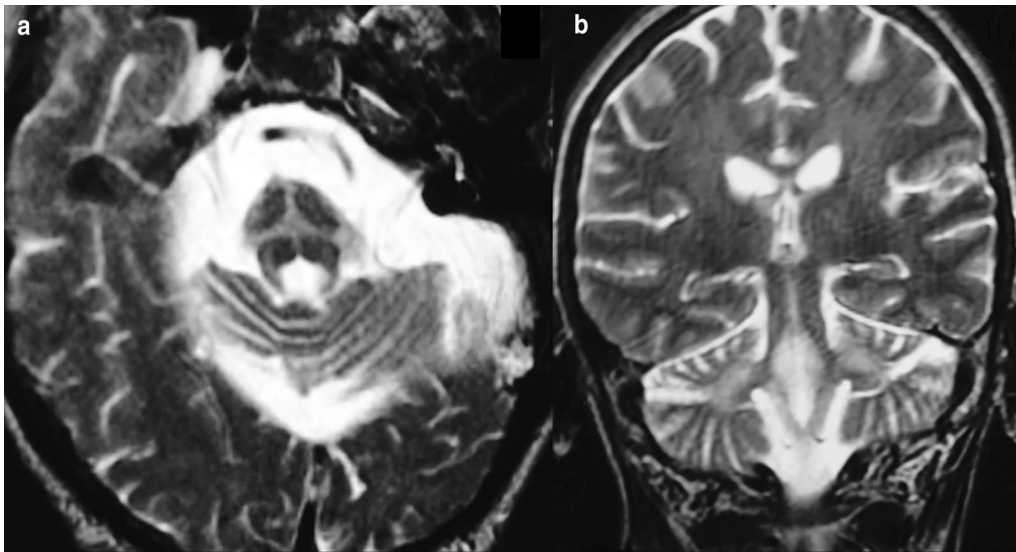


Fig. 15 Axial T2-weighted image demonstrates cruciform hyperintense signal in the pons, the so-called hot cross bun sign of MSA-C (a). Coronal T2-weighted image at the level of the brainstem demonstrates hyperintense signal in the bilateral brachis pontis, another common finding in the disease (b)

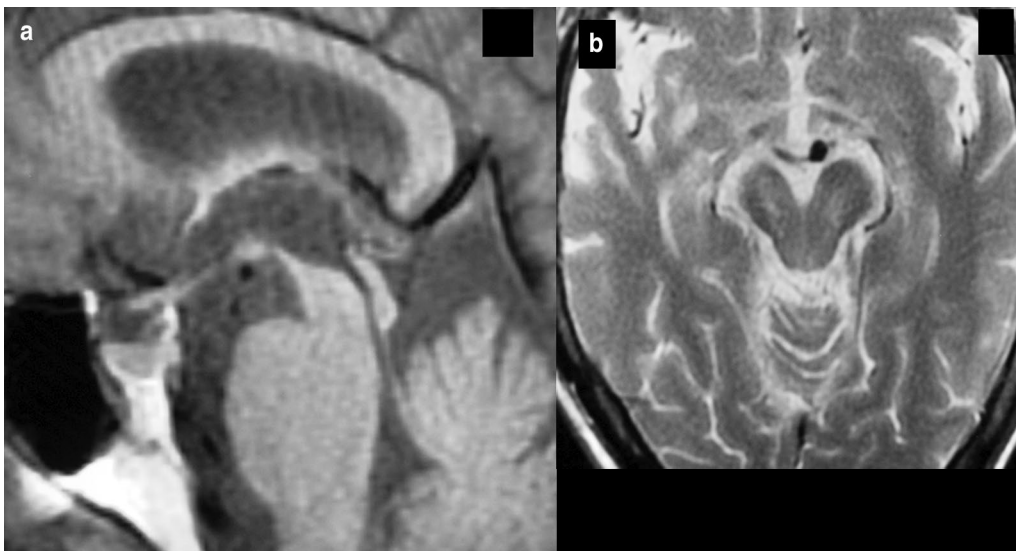


Fig. 16 Sagittal T1-weighted image in the midline coned to the brainstem demonstrates midbrain atrophy creating the so-called hummingbird sign of PSP (a). Axial T1-weighted image at the level of the midbrain demonstrates decrease in the AP dimension of the midbrain and widening of the interpeduncular cistern; the so-called morning glory sign (b)

brainstem and midline frontal cortex with a reported sensitivity of 60% and specificity of 96% by visual interpretation with significant augmentation of sensitivity when ss-SPM is added [179]. 18-Fluorine-PI-2620, which selectively binds to the 4R tau isoform, has shown promise as a biomarker in PSP, though further evaluation is warranted [187]. Single-photon emission computed tomography imaging of pre- and postsynaptic striatal neuronal

degeneration shows similar patterns to and is not able to reliably differentiate PD from PSP [188].

Corticobasal degeneration is a specific form of the corticobasal syndrome (CBS) defined by extrapyramidal symptoms which are often asymmetric including an “alien limb” phenomenon with later onset loss of multi-domain cognitive functioning with preserved episodic memory and poor response to levodopa therapy [189,

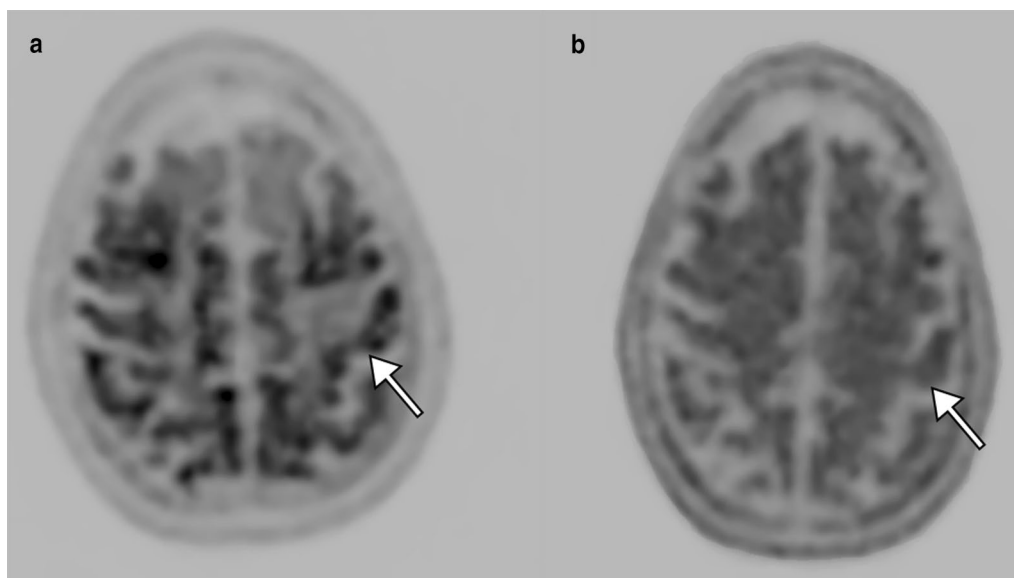


Fig. 17 A 60-year-old female with cognitive decline (MoCA 19/30) and limb apraxia. Flortaucipir PET/CT (**a**) demonstrates tau retention in the bilateral perirolandic regions (arrow indicating left precentral gyrus). Florbeta-PIR PET/CT (**b**) demonstrates radiotracer activity in the bilateral perirolandic regions (arrow indicating left precentral gyrus). Final diagnosis was CBS secondary to underlying AD, given the abnormal amyloid binding

[190]. Pathologically CBD is primarily a 4R tauopathy which demonstrates ballooned neurons in many areas of brain including the primary cortices as well as the cingulate gyrus, amygdala, insular cortex, and claustrum [191]. Typical structural MRI findings include asymmetric atrophy of the posterior frontal and parietal lobes contralateral to the patient's symptoms with associated atrophy of the contralateral cerebral peduncle and subcortical T2 FLAIR hyperintensity with relative preservation of basal ganglia volume and signal [174, 175, 192]. Reduced FA has been reported in the pre- and post-central gyri, cingulum, and supplementary motor area [193]. Resting-state functional MRI has documented hypoconnectivity of the lateral visual and auditory networks and hyperconnectivity of the salience and executive control networks [186]. Fluorodeoxyglucose PET shows similar findings with hypometabolism involving the primary cortices and additionally basal ganglia contralateral to the affected side [179, 194, 195]. Early research on Tau tracers for CBD has shown mixed results with 18-F-AV-1451,

18-F-PI-2620 may be a more appropriate tracer given its affinity for the 4R tau isoform [196–198]. The role of amyloid labeled tracers is uncertain given the overlap of CBS secondary to other dementias and imperfect tau isoform selectivity of current radiotracers (Fig. 17) [198]. Iodine-123-FP-CIT SPECT demonstrates asymmetric decreased striatal uptake with less disproportionate involvement of the putamen when compared to other Parkinsonian syndromes [199, 200]. Table 3 describes the common imaging features of parkinsonian syndromes.

Miscellaneous syndromes

Cerebral amyloid angiopathy

Cerebral amyloid angiopathy (CAA) is a disease of A β deposition in the walls of primarily the small cortical and leptomeningeal arteries and arterioles favoring the posterior regions [201, 202]. Approximately 10–20% of intracerebral hemorrhage at autopsy may be attributed to CAA with up to 80% of patients with CAA demonstrating concurrent AD pathology [203]. The updated Boston

(See figure on next page.)

Fig. 18 A 81-year-old female with a gradual decline in short term memory and depression. Susceptibility-weighted image demonstrates numerous subcortical microhemorrhages (**a**). Fluorodeoxyglucose PET/MRI (**b**) demonstrates relatively normal cerebral metabolism. Later she presented with an acute worsening of symptoms including new right-side weakness and dysphasia. Magnetic resonance imaging demonstrated T2 FLAIR hyperintensity within the left frontal lobe (**c**) without restricted diffusion (**d**). Final diagnosis was amyloid beta-related angiitis. Cognitive function improved following administration of steroids. Fluorodeoxyglucose PET/MRI suggested against concurrent AD. Images from a separate patient demonstrate occipito-temporal subcortical microhemorrhages (**e**) with diffuse amyloid uptake on florbeta-PIR PET/CT, a pattern suggesting concurrent CAA with AD (**f**)

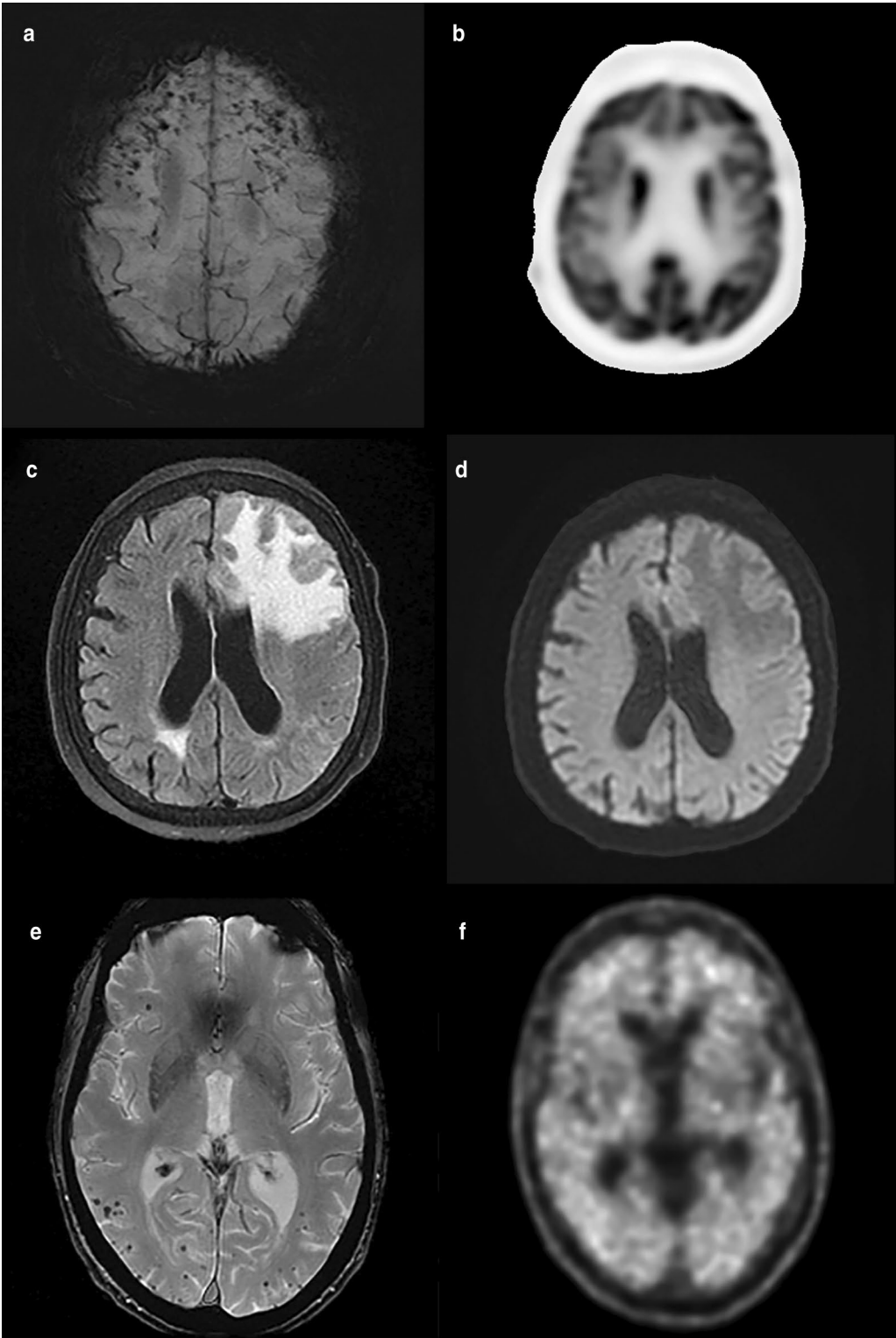


Fig. 18 (See legend on previous page.)

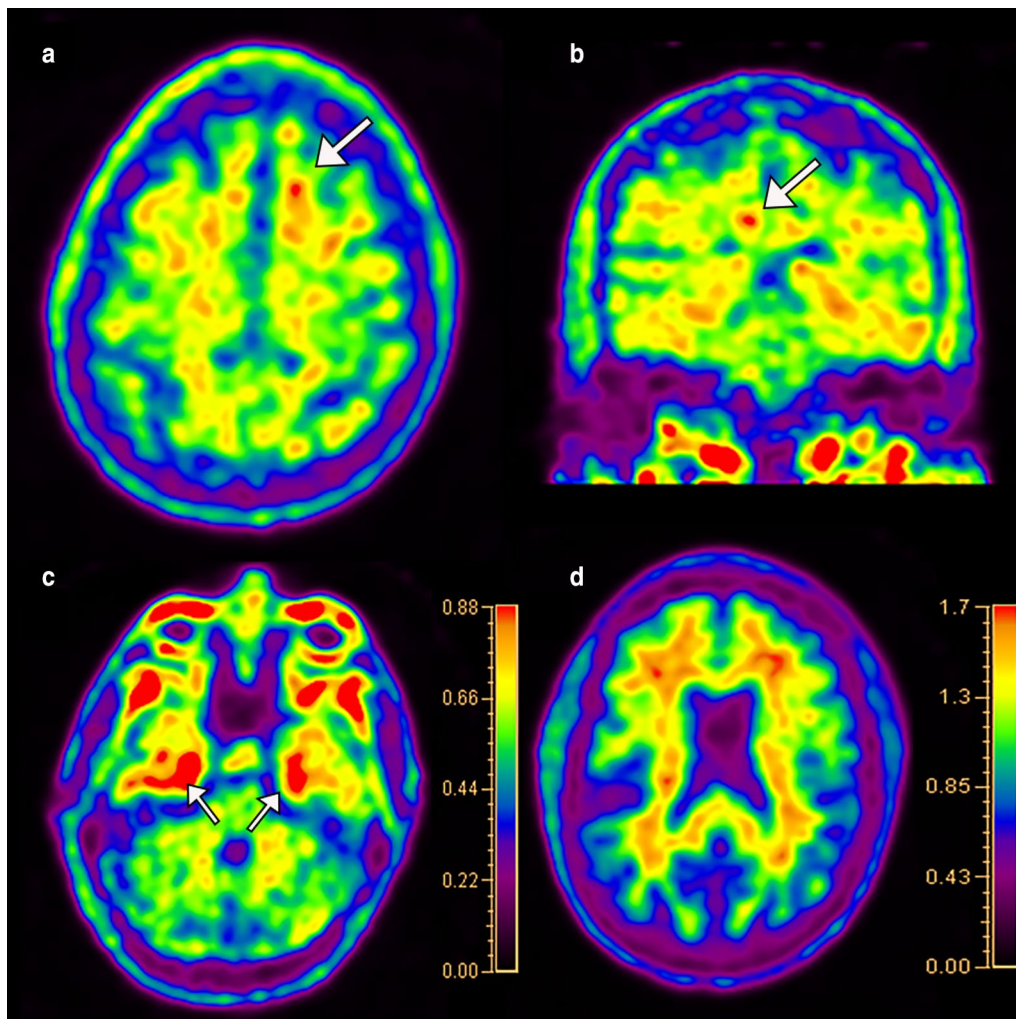


Fig. 19 A 70-year-old man with history of military combat and traumatic brain injury with MCI, MoCA 26/30. Flortaucipir PET/CT demonstrates regions of tau retention in the sulcal depths of the parasagittal frontal cortices (arrows in **a** and **b**). Tau retention is also noted in the bilateral mesial temporal lobes (arrows in **c**). Florbetapir PET/CT (**d**) demonstrates no significant cortical amyloid uptake involving the parietal lobes. Given the findings on PET/CT memory impairment was diagnosed as related to CTE

criteria 2.0, which includes findings on structural MRI of at least two either lobar or subcortical hemorrhagic lesions or scattered superficial siderosis or one of the aforementioned hemorrhagic lesions with greater than 20 perivascular spaces or white matter hyperintensities in one hemisphere without evidence of deep hemorrhagic lesions or evidence of other cause, was reported to have 64.5% sensitivity and 95% specificity for the diagnosis of typical CAA [204]. There are two rarer subtypes of CAA, inflammatory CAA, characterized by lobar edema with overlying leptomeningeal enhancement and subcortical microhemorrhages without diffusion restriction and amyloidoma, characterized by a solitary enhancing mass with surrounding edema (Fig. 18) [205]. One study demonstrated amyloid PET has good sensitivity

to discriminate CAA from controls, however, with modest specificity (sensitivity of 91% and specificity of 55%) [206]. The poor specificity of amyloid PET for the diagnosis of CAA is attributed to the overlap with AD pathology; the posterior predominance of CAA has led to reports of the occipital-to-posterior cingulate or global ratio as a possible means of discrimination from AD [207, 208]. Fluorodeoxyglucose PET has demonstrated similar findings with decrease in SUVr ratio of the occipital lobe relative to the PCC in patients with CAA compared to AD [209]. As with AD, early reports of tau agents in CAA have demonstrated increased binding correlated with worsening cognition, which was not demonstrated with amyloid agents [210].



Fig. 20 Coronal T1-weighted image demonstrates atrophy of the bilateral caudate heads with “box-shaped” ventricles

Chronic traumatic encephalopathy

Chronic traumatic encephalopathy (CTE) is a tauopathy secondary to repetitive mild traumatic brain injury more recently described in the literature with clinical features of decreased attention and memory, affective disturbances, psychosis, and gait and speech difficulties [211, 212]. Four progressive pathologic stages of the disease are defined with perivascular hyperphosphorylated tau NFTs beginning in the dorsolateral frontal cortices and spreading to the temporal and parietal lobes and deep nuclei with sparing of the calcarine cortex except in severe cases [213]. Amyloid plaques are not considered a feature of the disease [211]. Structural imaging shows an exceedingly higher than expected number of patients with a cavum septum pellucidum, felt to be related to shear forces due to a CSF fluid wave from trauma [213, 214]. Additionally, generalized cerebral white and gray matter volume loss has been reported [214, 215]. Reduced FA in white matter tracts including the superior and inferior longitudinal fasciculus, corona radiata, cerebral peduncle, uncinate fasciculus, and anterior thalamic radiations as well as the ventral striatum has been described [216–218]. Tau radiotracers are reported to have increased uptake in the frontotemporal lobes including the medial temporal lobes with frontal-lobe predominant involvement of the sulcal depths (Fig. 19) [219, 220]. Areas of hypometabolism on FDG-PET generally mirror the regions of tau retention [215, 220]. Variable positivity has been seen with amyloid tracers [219].

Amyotrophic lateral sclerosis

Amyotrophic lateral sclerosis (ALS) is a progressive neurodegenerative disorder characterized primarily by upper and lower motor neuron degeneration leading to clinical signs of progressive weakness, muscle atrophy, and fasciculations starting in the limbs [221]. The pathologic hallmark of the disease is ubiquitinated TDP-43 inclusions [222]. T2 hyperintensity involving the corticospinal tracts (CSTs) was one of the earliest reported imaging features of ALS; however, studies have demonstrated inconsistency in this finding [223–225]. Reduced FA on DTI and NAA on MR spectroscopy in the CSTs has been consistently reported [226, 227]. Increased iron deposition quantified by T2* imaging has been shown in the motor cortex of patients with ALS [228]. Resting-state functional MRI shows decreased connectivity in the motor network [229]. Fluorodeoxyglucose PET imaging has demonstrated hypometabolism in the motor/perirolandic and frontal cortices as well as the occipital lobes with a sensitivity of 94.8–95.4% and specificity of 80–82.5% for the diagnosis [230, 231]. Binding in the CSTs of 2-([1E,3E]-4-[6-([11C]methylamino)pyridinyl]buta-1,3-dienyl)benzo[d]thiazol-6-ol ([11C]PBB3), a tau radiotracer, was shown to correlate with upper motor neuron signs in a patient with ALS/parkinsonian dementia complex overlap; however, extensive reports of tau agents are lacking at the current time, although an attractive target given the pathologic findings of TDP-43 in ALS [222, 232].

Huntington’s disease

Huntington’s disease is an autosomal dominant neurodegenerative disorder characterized clinically by chorea, dementia, and psychosis, genetically by CAG trinucleotide repeat expansion on chromosome 4, and pathologically by atrophy in the striatum with involvement of other subcortical and cortical regions at higher stages [233]. Structural imaging shows striking atrophy of the striatum with ex vacuo dilation of the frontal horns of the lateral ventricles (so-called box-shaped ventricles), which is predictive of symptom onset (Fig. 20) [234]. Studies have overall demonstrated increased FA, felt to be related to selective neuronal degeneration (i.e. as selected tracts are damaged the remaining fibers demonstrate more organization), and increased MD in the basal ganglia [235]. Additional regions with reduced FA and increased MD include the CSTs and corpus callosum [235]. Hypometabolism in the striatum as well as the frontal and temporal lobes has been reported, with striatal hypometabolism a potential marker of time to symptom onset [236]. Decreased striatal dopamine receptor binding,

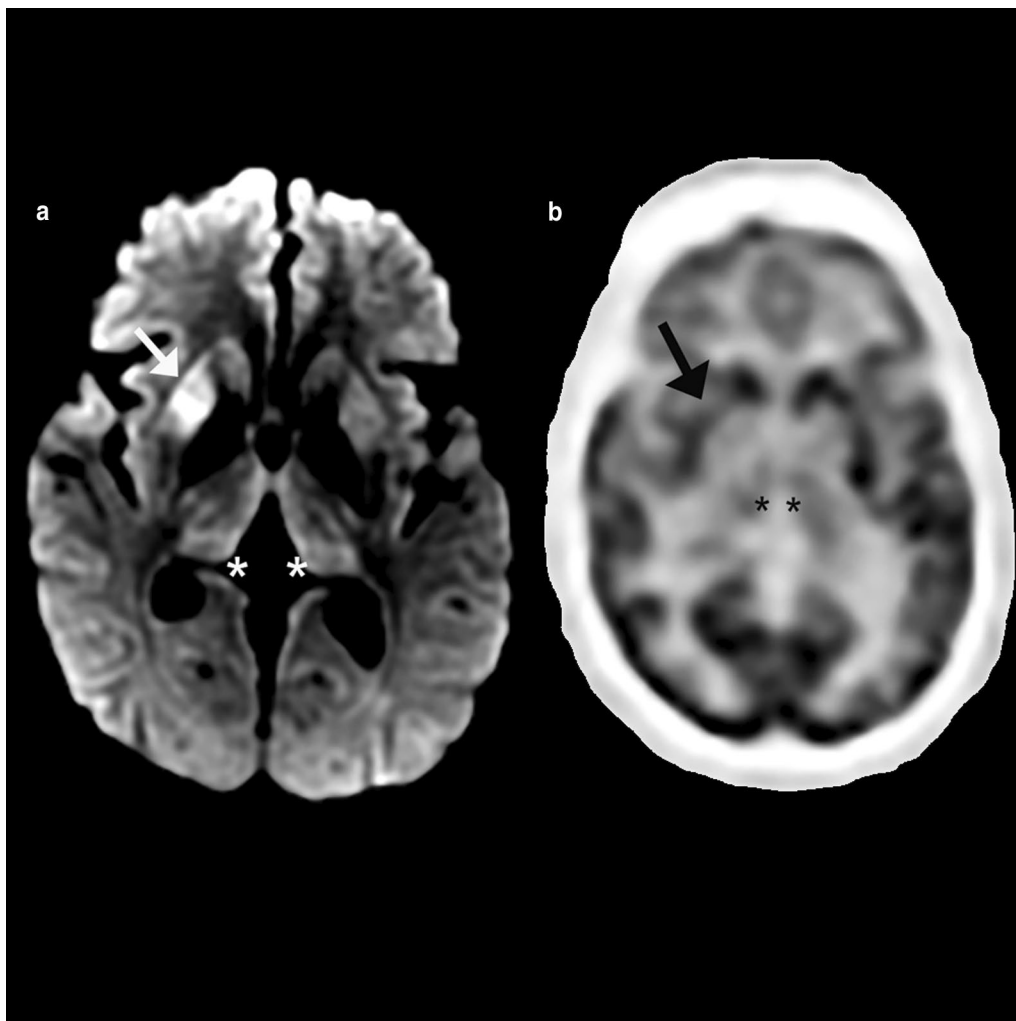


Fig. 21 A 64-year-old female with three months of progressive functional decline, failure to thrive, and weakness. Diffusion-weighted imaging (a) demonstrates hyperintensity in the right caudate head and lentiform nucleus (arrow) and the bilateral thalami with an L-shaped or “hockey stick” configuration (asterisks). Fluorodeoxyglucose PET/MRI (b) demonstrates corresponding asymmetric hypometabolism in the right lentiform nucleus (arrow) and bilateral thalami (asterisks). Cerebrospinal fluid 14-3-3 protein was positive and pathological examination of the brain was consistent with CJD

most commonly utilizing [^{11}C]raclopride-PET, has been exhibited in HD patients [237]. Other research targets have included adenosine, cannabinoid, and gamma-aminobutyric acid (GABA) receptors (diminished in HD), microglial activation (increased), phosphodiesterase 10A enzymatic activity (decreased), and synaptic vesicle protein 2A expression (decreased), all of which are not yet utilized clinically [238]. To date, a radiotracer targeting the Huntington protein is not available; however, this would obviously be an attractive target.

Creutzfeldt–Jakob disease

Creutzfeldt–Jakob disease (CJD) is a rapidly progressive uniformly fatal prion-driven NDD afflicting approximately 1–2 persons per million worldwide, with three subtypes,

the sporadic subtype representing the majority of cases [239]. Characteristic MRI features include hyperintensity on T2 or diffusion-weighted imaging (DWI) involving the cortex (cortical ribboning) and basal ganglia with involvement of the thalamus (“hockey stick sign”) less commonly reported in the sporadic subtype and more common in variant CJD (Fig. 21) [240]. T1 hyperintensity in the globus pallidus, thought to be related to accumulation of misfolded proteins, may also be observed, even without DWI changes [241]. Decreased NAA on MR spectroscopy has been reported and is likely related to neuronal death [242]. Asymmetric hypometabolism in the frontal and parietal cortices with or without decreased activity in the basal ganglia has been demonstrated with FDG-PET (Fig. 21) [243, 244]. Sporadic case reports have shown no significant

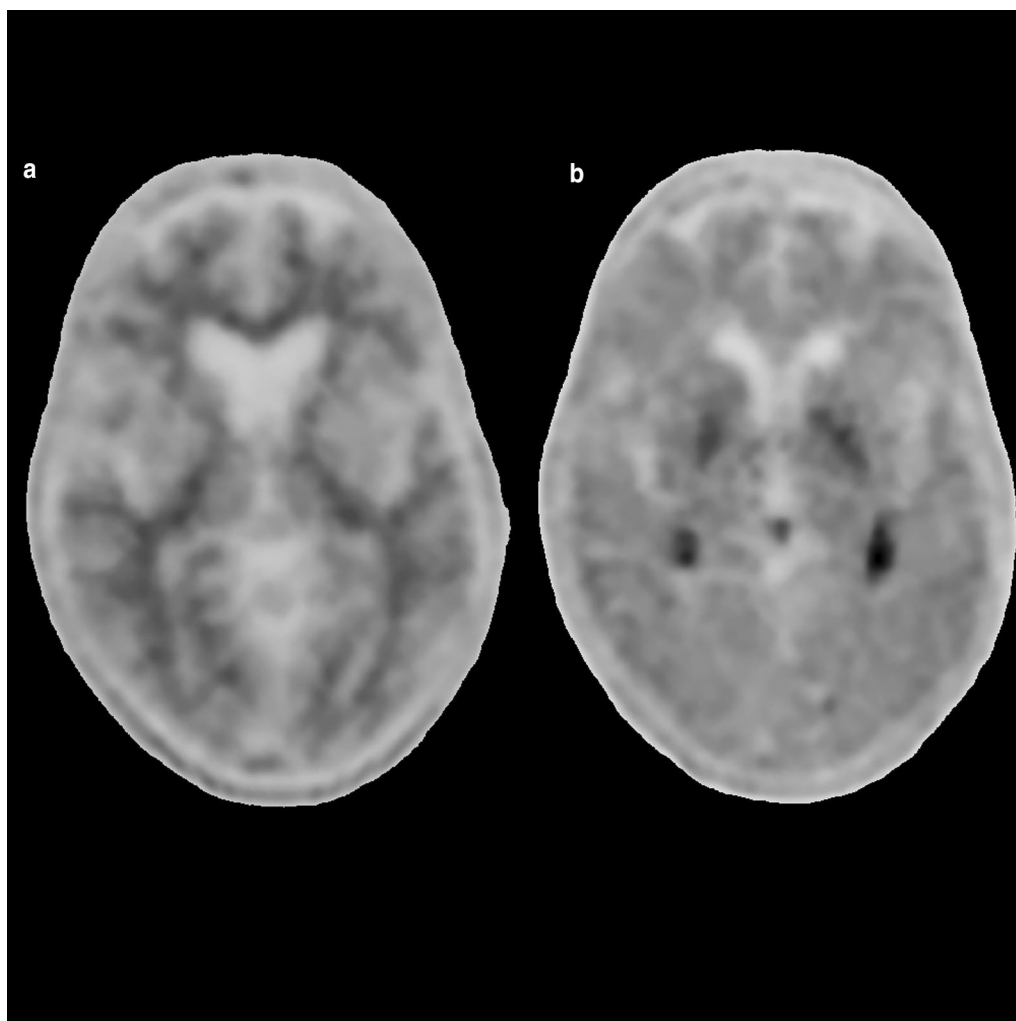


Fig. 22 A 65-year-old female with reported gradual decline in short term memory and depressive symptoms, initial MoCA 25/30. Florbetapir PET/CT demonstrates normal white matter distribution with no regions of abnormal cortical uptake, compatible with no to sparse amyloid plaque (**a**). Flortaucipir PET/CT demonstrates no cortical tau retention with off-target binding in the bilateral choroid plexuses and basal ganglia (**b**). Score on MoCA improved to 29/30 on antidepressant therapy. Final diagnosis was pseudodementia related to major depressive disorder

amyloid and F-18 flortaucipir retention with one case demonstrating uptake of 18F-THK5351, felt to be related to off-target binding of MAO-B activation in astrocytosis and correlating to the areas of signal abnormality [245–248].

Pseudodementia

Technically a non-NDD, pseudodementia was first described in 1961 by Kiloh as a condition of apparent dementia most commonly to a secondary mental illness such as depression leading to memory loss of recent and remote events and inattention [249, 250]. Often a geriatric depression scale is performed with initial memory care clinic consultation to exclude concomitant mental illness driving dementia symptoms [251]. Molecular imaging provides an excellent method to discriminate

non-NDDs/pseudodementia from NDDs (Fig. 22) [252, 253]. Table 4 describes the common imaging features of miscellaneous NDDs.

Conclusion

A wide variety of advanced multiparametric MRI and molecular imaging techniques are now available to increase diagnostic confidence of neurodegenerative syndromes, with ongoing research to thrust more of these techniques into a wider clinical role. Combined PET/MRI is an attractive imaging modality to provide a comprehensive workup of NDDs in a single imaging session. Ultimately, these techniques may be of use in selecting for and following up patients on monoclonal antibody therapy.

Abbreviations

11C-DED	11C-deuterium-l-deprenyl
3R	Three repeat
4R	Four repeat
AD	Alzheimer's disease
ARIAs	Amyloid-related imaging abnormalities
ASL	Arterial spin labeling
A β	Amyloid-beta
C-11	Carbon-11
C9ORF72	Chromosome 9 open reading frame 72
CAA	Cerebral amyloid angiopathy
CBD	Corticobasal degeneration
CBS	Corticobasal syndrome
CJD	Creutzfeldt–Jakob disease
CMRgluc	Cerebral metabolic rate of glucose
CTE	Chronic traumatic encephalopathy
CTSs	Corticospinal tracts
DAT	Dopamine transporter
DLB	Dementia with Lewy bodies
DMN	Default mode network
DTI	Diffusion tensor imaging
DWI	Diffusion-weighted imaging
F-18	Fluorine-18
FA	Fractional anisotropy
FDG-PET	2-[18F]fluoro-2-deoxy-d-glucose positron emission tomography
FTD	Frontotemporal dementia
FTLD	Frontotemporal lobar degeneration
FUS	Fused-in-sarcoma
I-123-FP-CIT, DaTSCAN	Iodine-123 N- ω -fluoropropyl-2 β -carboxymethoxy-3 β -[4-iodophenyl] nortropane
LC	Locus coeruleus
lvPPA	Logopenic variant primary progressive aphasia
MAO	Monoamine oxidase
MAPT	Microtubule-associated protein tau
MCI	Mild cognitive impairment
MD	Mean diffusivity
MMSE	Mini-mental state examination
MoCA	Montreal cognitive assessment
MRE	Magnetic resonance elastography
MRI	Magnetic resonance imaging
MSA	Multisystem atrophy
MSA-C	Multisystem atrophy with dominant cerebellar dysfunction
MSA-P	Multisystem atrophy with parkinsonian features
MTI	Magnetization transfer imaging
MTR	Magnetization transfer ratio
NAA	N-acetylaspartate
NDD	Neurodegenerative diseases
nfPPA	Nonfluent/agrammatic primary progressive aphasia
NFTs	Neurofibrillary tangles
PCA	Posterior cortical atrophy
PCC	Posterior cingulate cortex
PD	Parkinson's disease
PDD	PD-related dementia
PiB	Pittsburgh compound B
PSEN1	Presenilin 1
PSEN2	Presenilin 2
PSP	Progressive supranuclear palsy
ROI	Region of interest
rsfMRI	Resting-state functional MRI
SPECT	Single-photon emission computed tomography
ss-SPM	Single-subject statistical parametric mapping
SUVgluc	Standard uptake value of glucose
SUVr	Standardized uptake value ratio
svPPA	Semantic primary progressive aphasia
TDP-43	TAR DNA-binding protein 43
VaD	Vascular dementia
WMHs	White matter abnormalities/hyperintensities

Acknowledgements

We thank Sarah Klingenberger, Radiology Graphics Imaging Specialist at the University of Rochester Medical Center, and Kevin Hopkins, CNMT, for their assistance with preparing the figures for print.

Author contributions

JL was the major contributor in writing the manuscript. SP and SM contributed to the radiologic images and critically reviewed and revised the manuscript. All authors read and approved the final manuscript.

Funding

Not applicable.

Availability of data and materials

Not applicable.

Declarations**Ethics approval and consent to participate**

As the images contain no PHI, ethics approval is waived by the research subjects review board at the University of Rochester.

Consent for publication

Not applicable.

Competing interests

The authors declare that they have no competing interests.

Received: 17 August 2022 Accepted: 13 December 2022

Published online: 16 January 2023

References

- Cao Q, Tan CC, Xu W et al (2020) The prevalence of dementia: a systematic review and meta-analysis. *J Alzheimers Dis* 73:1157–1166. <https://doi.org/10.3233/jad-191092>
- Beach TG, Monsell SE, Phillips LE, Kukull W (2012) Accuracy of the clinical diagnosis of Alzheimer disease at National Institute on aging Alzheimer Disease Centers, 2005–2010. *J Neuropathol Exp Neurol* 71:266–273. <https://doi.org/10.1097/NEN.0b013e31824b211b>
- Salloway S, Sperling R, Fox NC et al (2014) Two phase 3 trials of bapineuzumab in mild-to-moderate Alzheimer's disease. *N Engl J Med* 370:322–333. <https://doi.org/10.1056/NEJMoa1304839>
- Vandenberghe R, Rinne JO, Boada M et al (2016) Bapineuzumab for mild to moderate Alzheimer's disease in two global, randomized, phase 3 trials. *Alzheimers Res Ther* 8:18. <https://doi.org/10.1186/s13195-016-0189-7>
- Sevigny J, Chiao P, Bussière T et al (2016) The antibody aducanumab reduces A β plaques in Alzheimer's disease. *Nature* 537:50–56. <https://doi.org/10.1038/nature19323>
- Honig LS, Vellas B, Woodward M et al (2018) Trial of Solanezumab for mild dementia due to Alzheimer's disease. *N Engl J Med* 378:321–330. <https://doi.org/10.1056/NEJMoa1705971>
- McKhann GM, Knopman DS, Chertkow H et al (2011) The diagnosis of dementia due to Alzheimer's disease: recommendations from the National Institute on Aging–Alzheimer's Association workgroups on diagnostic guidelines for Alzheimer's disease. *Alzheimers Dement* 7:263–269. <https://doi.org/10.1016/j.jalz.2011.03.005>
- Park M, Moon WJ (2016) Structural MR imaging in the diagnosis of Alzheimer's disease and other neurodegenerative dementia: current imaging approach and future perspectives. *Korean J Radiol* 17:827–845. <https://doi.org/10.3348/kjr.2016.17.6.827>
- Zukotynski K, Kuo PH, Mikulis D et al (2018) PET/CT of dementia. *AJR Am J Roentgenol* 211:246–259. <https://doi.org/10.2214/ajr.18.19822>
- Braak H, Braak E (1991) Neuropathological staging of Alzheimer-related changes. *Acta Neuropathol* 82:239–259. <https://doi.org/10.1007/bf00308809>

11. Braak H, Alafuzoff I, Arzberger T, Kretschmar H, Del Tredici K (2006) Staging of Alzheimer disease-associated neurofibrillary pathology using paraffin sections and immunocytochemistry. *Acta Neuropathol* 112:389–404. <https://doi.org/10.1007/s00401-006-0127-z>
12. Laforce R Jr, Soucy JP, Sellami L et al (2018) Molecular imaging in dementia: past, present, and future. *Alzheimers Dement* 14:1522–1552. <https://doi.org/10.1016/j.jalz.2018.06.2855>
13. Duara R, Loewenstein DA, Potter E et al (2008) Medial temporal lobe atrophy on MRI scans and the diagnosis of Alzheimer disease. *Neurology* 71:1986–1992. <https://doi.org/10.1212/01.wnl.0000336925.79704.9f>
14. Urs R, Potter E, Barker W et al (2009) Visual rating system for assessing magnetic resonance images: a tool in the diagnosis of mild cognitive impairment and Alzheimer disease. *J Comput Assist Tomogr* 33:73–78. <https://doi.org/10.1097/RCT.0b013e31816373d8>
15. Wolk DA, Das SR, Mueller SG, Weiner MW, Yushkevich PA (2017) Medial temporal lobe subregional morphometry using high resolution MRI in Alzheimer's disease. *Neurobiol Aging* 49:204–213. <https://doi.org/10.1016/j.neurobiolaging.2016.09.011>
16. Xie L, Wisse LEM, Pluta J et al (2019) Automated segmentation of medial temporal lobe subregions on in vivo T1-weighted MRI in early stages of Alzheimer's disease. *Hum Brain Mapp* 40:3431–3451. <https://doi.org/10.1002/hbm.24607>
17. Hill DLG, Schwarz AJ, Isaac M et al (2014) Coalition against major diseases/European medicines agency biomarker qualification of hippocampal volume for enrichment of clinical trials in predementia stages of Alzheimer's disease. *Alzheimers Dement* 10:421–9.e3. <https://doi.org/10.1016/j.jalz.2013.07.003>
18. Tanpitukpongse TP, Mazurkowski MA, Ikhenia J, Petrella JR (2017) Predictive utility of marketed volumetric software tools in subjects at risk for Alzheimer disease: do regions outside the hippocampus matter? *AJNR Am J Neuroradiol* 38:546–552. <https://doi.org/10.3174/ajnr.A5061>
19. Salloway S, Chalkias S, Barkhof F et al (2022) Amyloid-related imaging abnormalities in 2 phase 3 studies evaluating aducanumab in patients With early Alzheimer disease. *JAMA Neurol* 79:13–21. <https://doi.org/10.1001/jamaneurol.2021.4161>
20. Sexton CE, Kalu UG, Filippini N, Mackay CE, Ebmeier KP (2011) A meta-analysis of diffusion tensor imaging in mild cognitive impairment and Alzheimer's disease. *Neurobiol Aging* 32(2322):e5-18. <https://doi.org/10.1016/j.neurobiolaging.2010.05.019>
21. Nir TM, Jahanshad N, Villalon-Reina JE et al (2013) Effectiveness of regional DTI measures in distinguishing Alzheimer's disease, MCI, and normal aging. *Neuroimage Clin* 3:180–195. <https://doi.org/10.1016/j.nicl.2013.07.006>
22. Ridha BH, Tozer DJ, Symms MR et al (2007) Quantitative magnetization transfer imaging in Alzheimer disease. *Radiology* 244:832–837. <https://doi.org/10.1148/radiol.2443061128>
23. Betts MJ, Cardenas-Blanco A, Kanowski M et al (2019) Locus coeruleus MRI contrast is reduced in Alzheimer's disease dementia and correlates with CSF A β levels. *Alzheimers Dement (Amst)* 11:281–285. <https://doi.org/10.1016/j.dadm.2019.02.001>
24. Colonna I, Koini M, Pirpamer L et al (2021) Microstructural tissue changes in Alzheimer disease brains: insights from magnetization transfer imaging. *AJNR Am J Neuroradiol* 42:688–693. <https://doi.org/10.3174/ajnr.A6975>
25. Braak H, Thal DR, Ghebremedhin E, Del Tredici K (2011) Stages of the pathologic process in Alzheimer disease: age categories from 1 to 100 years. *J Neuropathol Exp Neurol* 70:960–969. <https://doi.org/10.1097/NEN.0b013e318232a379>
26. Chen Y, Chen T, Hou R (2022) Locus coeruleus in the pathogenesis of Alzheimer's disease: a systematic review. *Alzheimers Dement (N Y)* 8:e12257. <https://doi.org/10.1002/trc2.12257>
27. Waragai M, Moriya M, Nojo T (2017) Decreased N-Acetyl Aspartate/Myo-inositol ratio in the posterior cingulate cortex shown by magnetic resonance spectroscopy may be one of the risk markers of preclinical Alzheimer's disease: A 7-year follow-up study. *J Alzheimers Dis* 60:1411–1427. <https://doi.org/10.3233/jad-170450>
28. Riederer I, Bohn KP, Preibisch C et al (2018) Alzheimer disease and mild cognitive impairment: integrated pulsed arterial spin-labeling MRI and (18)F-FDG PET. *Radiology* 288:198–206. <https://doi.org/10.1148/radiol.2018170575>
29. Badhwar A, Tam A, Dansereau C, Orban P, Hoffstaedter F, Bellec P (2017) Resting-state network dysfunction in Alzheimer's disease: a systematic review and meta-analysis. *Alzheimers Dement (Amst)* 8:73–85. <https://doi.org/10.1016/j.dadm.2017.03.007>
30. ElSheikh M, Arani A, Perry A et al (2017) MR elastography demonstrates unique regional brain stiffness patterns in dementias. *AJR Am J Roentgenol* 209:403–408. <https://doi.org/10.2214/ajr.16.17455>
31. Bloudek LM, Spackman DE, Blankenburg M, Sullivan SD (2011) Review and meta-analysis of biomarkers and diagnostic imaging in Alzheimer's disease. *J Alzheimers Dis* 26:627–645. <https://doi.org/10.3233/jad-2011-110458>
32. Silverman DH, Small GW, Chang CY et al (2001) Positron emission tomography in evaluation of dementia: regional brain metabolism and long-term outcome. *JAMA* 286:2120–2127. <https://doi.org/10.1001/jama.286.17.2120>
33. Smailigik N, Lafortune L, Kelly S, Hyde C, Brayne C (2018) 18F-FDG PET for prediction of conversion to Alzheimer's disease dementia in people with mild cognitive impairment: an updated systematic review of test accuracy. *J Alzheimers Dis* 64:1175–1194. <https://doi.org/10.3233/jad-171125>
34. Drzezga A, Lautenschlager N, Siebner H et al (2003) Cerebral metabolic changes accompanying conversion of mild cognitive impairment into Alzheimer's disease: a PET follow-up study. *Eur J Nucl Med Mol Imaging* 30:1104–1113. <https://doi.org/10.1007/s00259-003-1194-1>
35. Del Sole A, Clerici F, Chiti A et al (2008) Individual cerebral metabolic deficits in Alzheimer's disease and amnesic mild cognitive impairment: an FDG PET study. *Eur J Nucl Med Mol Imaging* 35:1357–1366. <https://doi.org/10.1007/s00259-008-0773-6>
36. Sanabria-Diaz G, Martínez-Montes E, Melle-García L (2013) Glucose metabolism during resting state reveals abnormal brain networks organization in the Alzheimer's disease and mild cognitive impairment. *PLoS One* 8:e68860. <https://doi.org/10.1371/journal.pone.0068860>
37. Herholz K, Carter SF, Jones M (2007) Positron emission tomography imaging in dementia. *Br J Radiol* 80:S160–S167. <https://doi.org/10.1259/bjrr.97295129>
38. Sawyer DM, Kuo PH (2018) "Occipital Tunnel" sign on FDG PET for differentiating dementias. *Clin Nucl Med* 43:e59–e61. <https://doi.org/10.1097/rlu.0000000000001925>
39. Levin F, Ferreira D, Lange C et al (2021) Data-driven FDG-PET subtypes of Alzheimer's disease-related neurodegeneration. *Alzheimers Res Ther* 13:49. <https://doi.org/10.1186/s13195-021-00785-9>
40. Gorno-Tempini ML, Hillis AE, Weintraub S et al (2011) Classification of primary progressive aphasia and its variants. *Neurology* 76:1006–1014. <https://doi.org/10.1212/WNL.0b013e31821103e6>
41. Bergeron D, Sellami L, Poulin S, Verret L, Bouchard RW, Laforce R Jr (2020) The behavioral/dysexecutive variant of Alzheimer's disease: a case series with clinical, neuropsychological, and FDG-PET characterization. *Dement Geriatr Cogn Disord* 49:518–525. <https://doi.org/10.1159/000511210>
42. Herholz K (2014) The role of PET quantification in neurological imaging: FDG and amyloid imaging in dementia. *Clin Transl Imaging* 2:321–330. <https://doi.org/10.1007/s40336-014-0073-z>
43. Hutchins GD, Holden JE, Koeppel RA, Halama JR, Gately SJ, Nickles RJ (1984) Alternative approach to single-scan estimation of cerebral glucose metabolic rate using glucose analogs, with particular application to ischemia. *J Cereb Blood Flow Metab* 4:35–40. <https://doi.org/10.1038/jcbfm.1984.5>
44. Huang SC (2000) Anatomy of SUV. Standardized uptake value. *Nucl Med Biol* 27:643–646. [https://doi.org/10.1016/s0969-8051\(00\)00155-4](https://doi.org/10.1016/s0969-8051(00)00155-4)
45. Langbaum JB, Chen K, Lee W et al (2009) Categorical and correlational analyses of baseline fluorodeoxyglucose positron emission tomography images from the Alzheimer's disease neuroimaging initiative (ADNI). *Neuroimage* 45:1107–1116. <https://doi.org/10.1016/j.neuroimage.2008.12.072>
46. Furst AJ, Rabinovici GD, Rostomian AH et al (2012) Cognition, glucose metabolism and amyloid burden in Alzheimer's disease. *Neurobiol Aging* 33:215–225. <https://doi.org/10.1016/j.neurobiolaging.2010.03.011>
47. Della Rosa PA, Cerami C, Gallivanone F et al (2014) A standardized [18F]-FDG-PET template for spatial normalization in statistical

- parametric mapping of dementia. *Neuroinformatics* 12:575–593. <https://doi.org/10.1007/s12021-014-9235-4>
48. Perani D, Della Rosa PA, Cerami C et al (2014) Validation of an optimized SPM procedure for FDG-PET in dementia diagnosis in a clinical setting. *Neuroimage Clin* 6:445–454. <https://doi.org/10.1016/j.nicl.2014.10.009>
 49. Ford JN, Sweeney EM, Skafida M et al (2021) Heuristic scoring method utilizing FDG-PET statistical parametric mapping in the evaluation of suspected Alzheimer disease and frontotemporal lobar degeneration. *Am J Nucl Med Mol Imaging* 11:313–326
 50. Klunk WE, Engler H, Nordberg A et al (2004) Imaging brain amyloid in Alzheimer's disease with Pittsburgh compound-B. *Ann Neurol* 55:306–319. <https://doi.org/10.1002/ana.20009>
 51. Yeo JM, Waddell B, Khan Z, Pal S (2015) A systematic review and meta-analysis of (18F)-labeled amyloid imaging in Alzheimer's disease. *Alzheimers Dement (Amst)* 1:5–13. <https://doi.org/10.1016/j.dadm.2014.11.004>
 52. Hellwig S, Frings L, Bormann T, Vach W, Buchert R, Meyer PT (2019) Amyloid imaging for differential diagnosis of dementia: incremental value compared to clinical diagnosis and [(18F)FDG PET. *Eur J Nucl Med Mol Imaging* 46:312–323. <https://doi.org/10.1007/s00259-018-4111-3>
 53. Clark CM, Schneider JA, Bedell BJ et al (2011) Use of florbetapir-PET for imaging beta-amyloid pathology. *JAMA* 305:275–283. <https://doi.org/10.1001/jama.2010.2008>
 54. Fodero-Tavoletti MT, Brockschneider D, Villemagne VL et al (2012) In vitro characterization of [18F]-florbetaben, an A β imaging radiotracer. *Nucl Med Biol* 39:1042–1048. <https://doi.org/10.1016/j.nucmedbio.2012.03.001>
 55. Buckley CJ, Sherwin PF, Smith AP, Wolber J, Weick SM, Brooks DJ (2017) Validation of an electronic image reader training programme for interpretation of [18F]flutemetamol β -amyloid PET brain images. *Nucl Med Commun* 38:234–241. <https://doi.org/10.1097/mnm.00000000000000633>
 56. Lundeen TF, Seibyl JP, Covington MF, Eshghi N, Kuo PH (2018) Signs and artifacts in amyloid PET. *Radiographics* 38:2123–2133. <https://doi.org/10.1148/rg.2018180160>
 57. Mormino EC, Brandel MG, Madison CM et al (2012) Not quite PIB-positive, not quite PIB-negative: slight PIB elevations in elderly normal control subjects are biologically relevant. *Neuroimage* 59:1152–1160. <https://doi.org/10.1016/j.neuroimage.2011.07.098>
 58. Palmqvist S, Zetterberg H, Mattsson N et al (2015) Detailed comparison of amyloid PET and CSF biomarkers for identifying early Alzheimer disease. *Neurology* 85:1240–1249. <https://doi.org/10.1212/wnl.000000000000001991>
 59. van Berckel BN, Ossenkoppele R, Tolboom N et al (2013) Longitudinal amyloid imaging using 11C-PIB: methodologic considerations. *J Nucl Med* 54:1570–1576. <https://doi.org/10.2967/jnumed.112.113654>
 60. Thurfjell L, Lilja J, Lundqvist R et al (2014) Automated quantification of 18F-flutemetamol PET activity for categorizing scans as negative or positive for brain amyloid: concordance with visual image reads. *J Nucl Med* 55:1623–1628. <https://doi.org/10.2967/jnumed.114.142109>
 61. Ng S, Villemagne VL, Berlangieri S et al (2007) Visual assessment versus quantitative assessment of 11C-PIB PET and 18F-FDG PET for detection of Alzheimer's disease. *J Nucl Med* 48:547–552. <https://doi.org/10.2967/jnumed.106.037762>
 62. Camus V, Payoux P, Barré L et al (2012) Using PET with 18F-AV-45 (florbetapir) to quantify brain amyloid load in a clinical environment. *Eur J Nucl Med Mol Imaging* 39:621–631. <https://doi.org/10.1007/s00259-011-2021-8>
 63. Akamatsu G, Ikari Y, Ohnishi A et al (2019) Voxel-based statistical analysis and quantification of amyloid PET in the Japanese Alzheimer's disease neuroimaging initiative (J-ADNI) multi-center study. *EJNMMI Res* 9:91. <https://doi.org/10.1186/s13550-019-0561-2>
 64. Raman F, Fang YD, Grandhi S et al (2022) Dynamic amyloid PET: relationships to (18F)-Flortaucipir tau PET measures. *J Nucl Med* 63:287–293. <https://doi.org/10.2967/jnumed.120.254490>
 65. Chien DT, Bahri S, Szardenings AK et al (2013) Early clinical PET imaging results with the novel PHF-tau radioligand [F-18]-T807. *J Alzheimers Dis* 34:457–468. <https://doi.org/10.3233/jad-122059>
 66. Baker SL, Harrison TM, Maass A, La Joie R, Jagust WJ (2019) Effect of off-target binding on (18F)-Flortaucipir variability in healthy controls across the life span. *J Nucl Med* 60:1444–1451. <https://doi.org/10.2967/jnumed.118.224113>
 67. Walji AM, Hostetler ED, Selnick H et al (2016) Discovery of 6-(Fluoro-18F)-3-(1H-pyrrolo[2,3-c]pyridin-1-yl)isoquinolin-5-amine ([18F]-MK-6240): a positron emission tomography (PET) imaging agent for quantification of neurofibrillary tangles (NFTs). *J Med Chem* 59:4778–4789. <https://doi.org/10.1021/acs.jmedchem.6b00166>
 68. Honer M, Gobbi L, Knust H et al (2018) Preclinical evaluation of 8F-RO6958948, 11C-RO6931643, and 11C-RO6924963 as Novel PET radiotracers for imaging tau aggregates in Alzheimer disease. *J Nucl Med* 59:675–681. <https://doi.org/10.2967/jnumed.117.196741>
 69. Leuzy A, Chiotis K, Lemoine L et al (2019) Tau PET imaging in neurodegenerative tauopathies-still a challenge. *Mol Psychiatry* 24:1112–1134. <https://doi.org/10.1038/s41380-018-0342-8>
 70. Sanabria Bohórquez S, Marik J, Ogasawara A et al (2019) [18F]GTP1 (Genentech Tau Probe 1), a radioligand for detecting neurofibrillary tangle tau pathology in Alzheimer's disease. *Eur J Nucl Med Mol Imaging* 46:2077–2089. <https://doi.org/10.1007/s00259-019-04399-0>
 71. Kroth H, Oden F, Molette J et al (2019) Discovery and preclinical characterization of [(18F)PI]-2620, a next-generation tau PET tracer for the assessment of tau pathology in Alzheimer's disease and other tauopathies. *Eur J Nucl Med Mol Imaging* 46:2178–2189. <https://doi.org/10.1007/s00259-019-04397-2>
 72. Gobbi LC, Knust H, Körner M et al (2017) Identification of three novel radiotracers for imaging aggregated tau in Alzheimer's disease with positron emission tomography. *J Med Chem* 60:7350–7370. <https://doi.org/10.1021/acs.jmedchem.7b00632>
 73. Hostetler ED, Walji AM, Zeng Z et al (2016) Preclinical characterization of 18F-MK-6240, a promising PET tracer for in vivo quantification of human neurofibrillary tangles. *J Nucl Med* 57:1599–1606. <https://doi.org/10.2967/jnumed.115.171678>
 74. Schöll M, Lockhart SN, Schonhaut DR et al (2016) PET imaging of tau deposition in the aging human brain. *Neuron* 89:971–982. <https://doi.org/10.1016/j.neuron.2016.01.028>
 75. Biel D, Brendel M, Rubinski A et al (2021) Tau-PET and in vivo Braak-staging as prognostic markers of future cognitive decline in cognitively normal to demented individuals. *Alzheimers Res Ther* 13:137. <https://doi.org/10.1186/s13195-021-00880-x>
 76. Fleisher AS, Pontecorvo MJ, Devous MD Sr et al (2020) Positron emission tomography imaging With [18F]flortaucipir and postmortem assessment of Alzheimer disease neuropathologic changes. *JAMA Neurol* 77:829–839. <https://doi.org/10.1001/jamaneurol.2020.0528>
 77. Ossenkoppele R, Schonhaut DR, Schöll M et al (2016) Tau PET patterns mirror clinical and neuroanatomical variability in Alzheimer's disease. *Brain* 139:1551–1567. <https://doi.org/10.1093/brain/aww027>
 78. Xia C, Makarets SJ, Caso C et al (2017) Association of In vivo [18F]AV-1451 tau PET imaging results with cortical atrophy and symptoms in typical and atypical Alzheimer disease. *JAMA Neurol* 74:427–436. <https://doi.org/10.1001/jamaneurol.2016.5755>
 79. Chiotis K, Saint-Aubert L, Rodriguez-Vieitez E et al (2018) Longitudinal changes of tau PET imaging in relation to hypometabolism in prodromal and Alzheimer's disease dementia. *Mol Psychiatry* 23:1666–1673. <https://doi.org/10.1038/mp.2017.108>
 80. Vemuri P, Lowe VJ, Knopman DS et al (2017) Tau-PET uptake: regional variation in average SUVR and impact of amyloid deposition. *Alzheimers Dement (Amst)* 6:21–30. <https://doi.org/10.1016/j.dadm.2016.12.010>
 81. Varrone A, Oikonen V, Forsberg A et al (2015) Positron emission tomography imaging of the 18-kDa translocator protein (TSPO) with [18F]FEMPA in Alzheimer's disease patients and control subjects. *Eur J Nucl Med Mol Imaging* 42:438–446. <https://doi.org/10.1007/s00259-014-2955-8>
 82. Santillo AF, Gambini JP, Lannfelt L et al (2011) In vivo imaging of astrocytosis in Alzheimer's disease: an ¹¹C-L-deuteriodesprenyl and PIB PET study. *Eur J Nucl Med Mol Imaging* 38:2202–2208. <https://doi.org/10.1007/s00259-011-1895-9>
 83. Edison P, Archer HA, Gerhard A et al (2008) Microglia, amyloid, and cognition in Alzheimer's disease: an [11C](R)PK11195-PET and [11C]PIB-PET

- study. *Neurobiol Dis* 32:412–419. <https://doi.org/10.1016/j.nbd.2008.08.001>
84. Wiley CA, Lopresti BJ, Venneri S et al (2009) Carbon 11-labeled Pittsburgh compound B and carbon 11-labeled (R)-PK11195 positron emission tomographic imaging in Alzheimer disease. *Arch Neurol* 66:60–67. <https://doi.org/10.1001/archneurol.2008.511>
 85. Yokokura M, Mori N, Yagi S et al (2011) In vivo changes in microglial activation and amyloid deposits in brain regions with hypometabolism in Alzheimer's disease. *Eur J Nucl Med Mol Imaging* 38:343–351. <https://doi.org/10.1007/s00259-010-1612-0>
 86. Schuitemaker A, Kropholler MA, Boellaard R et al (2013) Microglial activation in Alzheimer's disease: an (R)-[¹¹C]PK11195 positron emission tomography study. *Neurobiol Aging* 34:128–136. <https://doi.org/10.1016/j.neurobiolaging.2012.04.021>
 87. Carter SF, Schöll M, Almkvist O et al (2012) Evidence for astrogliosis in prodromal Alzheimer disease provided by 11C-deuterium-L-deprenyl: a multitracers PET paradigm combining 11C-Pittsburgh compound B and 18F-FDG. *J Nucl Med* 53:37–46. <https://doi.org/10.2967/jnumed.110.087031>
 88. Rodriguez-Vieitez E, Saint-Aubert L, Carter SF et al (2016) Diverging longitudinal changes in astrogliosis and amyloid PET in autosomal dominant Alzheimer's disease. *Brain* 139:922–936. <https://doi.org/10.1093/brain/aww404>
 89. Carter SF, Chiotis K, Nordberg A, Rodriguez-Vieitez E (2019) Longitudinal association between astrocyte function and glucose metabolism in autosomal dominant Alzheimer's disease. *Eur J Nucl Med Mol Imaging* 46:348–356. <https://doi.org/10.1007/s00259-018-4217-7>
 90. Warnock GI, Aerts J, Bahri MA et al (2014) Evaluation of 18F-UCB-H as a novel PET tracer for synaptic vesicle protein 2A in the brain. *J Nucl Med* 55:1336–1341. <https://doi.org/10.2967/jnumed.113.136143>
 91. Nabulsi NB, Mercier J, Holden D et al (2016) Synthesis and preclinical evaluation of 11C-UCB-J as a PET tracer for imaging the synaptic vesicle glycoprotein 2A in the brain. *J Nucl Med* 57:777–784. <https://doi.org/10.2967/jnumed.115.168179>
 92. Chen MK, Mecca AP, Naganawa M et al (2018) Assessing synaptic density in Alzheimer disease with synaptic vesicle glycoprotein 2A positron emission tomographic imaging. *JAMA Neurol* 75:1215–1224. <https://doi.org/10.1001/jama.2018.1836>
 93. Bastin C, Bahri MA, Meyer F et al (2020) In vivo imaging of synaptic loss in Alzheimer's disease with [18F]UCB-H positron emission tomography. *Eur J Nucl Med Mol Imaging* 47:390–402. <https://doi.org/10.1007/s00259-019-04461-x>
 94. Hogan DB, Fiest KM, Roberts JL et al (2016) The prevalence and incidence of dementia with Lewy bodies: a systematic review. *Can J Neurol Sci* 43(Suppl 1):S83–95. <https://doi.org/10.1017/cjn.2016.2>
 95. McKeith IG, Boeve BF, Dickson DW et al (2017) Diagnosis and management of dementia with Lewy bodies: Fourth consensus report of the DLB Consortium. *Neurology* 89:88–100. <https://doi.org/10.1212/wnl.0000000000004058>
 96. Tsuboi Y, Dickson DW (2005) Dementia with Lewy bodies and Parkinson's disease with dementia: are they different? *Parkinsonism Relat Disord* 11(Suppl 1):S47–51. <https://doi.org/10.1016/j.parkreldis.2004.10.014>
 97. Tsuang D, Leverenz JB, Lopez OL et al (2013) APOE ε4 increases risk for dementia in pure synucleinopathies. *JAMA Neurol* 70:223–228. <https://doi.org/10.1001/jama.2013.600>
 98. Elahi FM, Miller BL (2017) A clinicopathological approach to the diagnosis of dementia. *Nat Rev Neurol* 13:457–476. <https://doi.org/10.1038/nrneurol.2017.96>
 99. Burton EJ, Karas G, Paling SM et al (2002) Patterns of cerebral atrophy in dementia with Lewy bodies using voxel-based morphometry. *Neuroimage* 17:618–630
 100. Burton EJ, Barber R, Mukaetova-Ladinska EB et al (2009) Medial temporal lobe atrophy on MRI differentiates Alzheimer's disease from dementia with Lewy bodies and vascular cognitive impairment: a prospective study with pathological verification of diagnosis. *Brain* 132:195–203. <https://doi.org/10.1093/brain/awn298>
 101. Lebedev AV, Westman E, Beyer MK et al (2013) Multivariate classification of patients with Alzheimer's and dementia with Lewy bodies using high-dimensional cortical thickness measurements: an MRI surface-based morphometric study. *J Neurol* 260:1104–1115. <https://doi.org/10.1007/s00415-012-6768-z>
 102. Whitwell JL, Weigand SD, Shiung MM et al (2007) Focal atrophy in dementia with Lewy bodies on MRI: a distinct pattern from Alzheimer's disease. *Brain* 130:708–719. <https://doi.org/10.1093/brain/awl388>
 103. Bozzali M, Falini A, Cercignani M et al (2005) Brain tissue damage in dementia with Lewy bodies: an in vivo diffusion tensor MRI study. *Brain* 128:1595–1604. <https://doi.org/10.1093/brain/awh493>
 104. Firbank MJ, Blamire AM, Krishnan MS et al (2007) Atrophy is associated with posterior cingulate white matter disruption in dementia with Lewy bodies and Alzheimer's disease. *Neuroimage* 36:1–7. <https://doi.org/10.1016/j.neuroimage.2007.02.027>
 105. Kantarci K, Avula R, Senjem ML et al (2010) Dementia with Lewy bodies and Alzheimer disease: neurodegenerative patterns characterized by DTI. *Neurology* 74:1814–1821. <https://doi.org/10.1212/WNL.0b013e3181e0f7cf>
 106. Watson R, Blamire AM, Colloby SJ et al (2012) Characterizing dementia with Lewy bodies by means of diffusion tensor imaging. *Neurology* 79:906–914. <https://doi.org/10.1212/WNL.0b013e318266fc51>
 107. Firbank MJ, Watson R, Mak E et al (2016) Longitudinal diffusion tensor imaging in dementia with Lewy bodies and Alzheimer's disease. *Parkinsonism Relat Disord* 24:76–80. <https://doi.org/10.1016/j.parkreldis.2016.01.003>
 108. Shams S, Fällmar D, Schwarz S et al (2017) MRI of the swallow tail sign: a useful marker in the diagnosis of lewy body dementia? *AJNR Am J Neuroradiol* 38:1737–1741. <https://doi.org/10.3174/ajnr.A5274>
 109. Kamagata K, Nakatsuka T, Sakakibara R et al (2017) Diagnostic imaging of dementia with Lewy bodies by susceptibility-weighted imaging of nigrosomes versus striatal dopamine transporter single-photon emission computed tomography: a retrospective observational study. *Neuroradiology* 59:89–98. <https://doi.org/10.1007/s00234-016-1773-z>
 110. Kitao S, Matsusue E, Fujii S et al (2013) Correlation between pathology and neuromelanin MR imaging in Parkinson's disease and dementia with Lewy bodies. *Neuroradiology* 55:947–953. <https://doi.org/10.1007/s00234-013-1199-9>
 111. Madelung CF, Meder D, Fuglsang SA et al (2022) Locus coeruleus shows a spatial pattern of structural disintegration in Parkinson's disease. *Mov Disord* 37:479–489. <https://doi.org/10.1002/mds.28945>
 112. Lowther ER, O'Brien JT, Firbank MJ, Blamire AM (2014) Lewy body compared with Alzheimer dementia is associated with decreased functional connectivity in resting state networks. *Psychiatry Res* 223:192–201. <https://doi.org/10.1016/j.pscychresns.2014.06.004>
 113. Sourty M, Thoraval L, Roquet D, Armspach JP, Foucher J, Blanc F (2016) Identifying dynamic functional connectivity changes in dementia with Lewy bodies based on product hidden markov models. *Front Comput Neurosci* 10:60. <https://doi.org/10.3389/fncom.2016.00060>
 114. Marshall VL, Reiningner CB, Marquardt M et al (2009) Parkinson's disease is overdiagnosed clinically at baseline in diagnostically uncertain cases: a 3-year European multicenter study with repeat [123I]FP-CIT SPECT. *Mov Disord* 24:500–508. <https://doi.org/10.1002/mds.22108>
 115. O'Brien JT, Oertel WH, McKeith IG et al (2014) Is ioflupane I123 injection diagnostically effective in patients with movement disorders and dementia? Pooled analysis of four clinical trials. *BMJ Open* 4:e005122. <https://doi.org/10.1136/bmjopen-2014-005122>
 116. Thomas AJ, Attems J, Colloby SJ et al (2017) Autopsy validation of 123I-FP-CIT dopaminergic neuroimaging for the diagnosis of DLB. *Neurology* 88:276–283. <https://doi.org/10.1212/wnl.0000000000003512>
 117. King AE, Mintz J, Royall DR (2011) Meta-analysis of 123I-MIBG cardiac scintigraphy for the diagnosis of Lewy body-related disorders. *Mov Disord* 26:1218–1224. <https://doi.org/10.1002/mds.23659>
 118. Yoshita M, Taki J, Yamada M (2001) A clinical role for [¹²³I]MIBG myocardial scintigraphy in the distinction between dementia of the Alzheimer's-type and dementia with Lewy bodies. *J Neurol Neurosurg Psychiatry* 71:583. <https://doi.org/10.1136/jnnp.71.5.583>
 119. Klein JC, Eggers C, Kalbe E et al (2010) Neurotransmitter changes in dementia with Lewy bodies and Parkinson disease dementia in vivo. *Neurology* 74:885–892. <https://doi.org/10.1212/WNL.0b013e3181d55f61>
 120. Lim SM, Katsifis A, Villemagne VL et al (2009) The 18F-FDG PET cingulate island sign and comparison to 123I-beta-CIT SPECT for diagnosis of

- dementia with Lewy bodies. *J Nucl Med* 50:1638–1645. <https://doi.org/10.2967/jnumed.109.065870>
121. Rowe CC, Ng S, Ackermann U et al (2007) Imaging beta-amyloid burden in aging and dementia. *Neurology* 68:1718–1725. <https://doi.org/10.1212/01.wnl.0000261919.22630.ea>
122. Gomperts SN, Rentz DM, Moran E et al (2008) Imaging amyloid deposition in Lewy body diseases. *Neurology* 71:903–910. <https://doi.org/10.1212/01.wnl.0000326146.60732.d6>
123. Edison P, Rowe CC, Rinne JO et al (2008) Amyloid load in Parkinson's disease dementia and Lewy body dementia measured with [11C] PIB positron emission tomography. *J Neurol Neurosurg Psychiatry* 79:1331–1338. <https://doi.org/10.1136/jnnp.2007.127878>
124. Gomperts SN, Locascio JJ, Marquie M et al (2012) Brain amyloid and cognition in Lewy body diseases. *Mov Disord* 27:965–973. <https://doi.org/10.1002/mds.25048>
125. Albin RL, Fisher-Hubbard A, Shanmugasundaram K et al (2015) Post-Mortem evaluation of amyloid-dopamine terminal positron emission tomography dementia classifications. *Ann Neurol* 78:824–830. <https://doi.org/10.1002/ana.24481>
126. Gomperts SN, Locascio JJ, Makarewicz SJ et al (2016) Tau positron emission tomographic imaging in the Lewy body diseases. *JAMA Neurol* 73:1334–1341. <https://doi.org/10.1001/jamaneurol.2016.3338>
127. Kantarci K, Lowe VJ, Boeve BF et al (2017) AV-1451 tau and β -amyloid positron emission tomography imaging in dementia with Lewy bodies. *Ann Neurol* 81:58–67. <https://doi.org/10.1002/ana.24825>
128. Fodero-Tavoletti MT, Mulligan RS, Okamura N et al (2009) In vitro characterisation of BF227 binding to alpha-synuclein/Lewy bodies. *Eur J Pharmacol* 617:54–58. <https://doi.org/10.1016/j.ejphar.2009.06.042>
129. Zhang X, Jin H, Padakanti PK et al (2014) Radiosynthesis and in vivo evaluation of two PET radioligands for imaging α -synuclein. *Appl Sci (Basel)* 4:66–78. <https://doi.org/10.3390/app4010066>
130. Chu W, Zhou D, Gaba V et al (2015) Design, synthesis, and characterization of 3-(Benzylidene)indolin-2-one derivatives as ligands for α -synuclein fibrils. *J Med Chem* 58:6002–6017. <https://doi.org/10.1021/acs.jmedchem.5b00571>
131. Plassman BL, Langa KM, Fisher GG et al (2007) Prevalence of dementia in the United States: the aging, demographics, and memory study. *Neuroepidemiology* 29:125–132. <https://doi.org/10.1159/000109998>
132. Sachdev PS, Brodaty H, Valenzuela MJ et al (2004) The neuropsychological profile of vascular cognitive impairment in stroke and TIA patients. *Neurology* 62:912–919. <https://doi.org/10.1212/01.wnl.0000115108.65264.4b>
133. de Groot JC, de Leeuw FE, Oudkerk M, Hofman A, Jolles J, Breteler MM (2000) Cerebral white matter lesions and depressive symptoms in elderly adults. *Arch Gen Psychiatry* 57:1071–1076. <https://doi.org/10.1001/archpsyc.57.11.1071>
134. Román GC, Tatemichi TK, Erkinjuntti T et al (1993) Vascular dementia: diagnostic criteria for research studies. Report of the NINDS-AIREN International Workshop. *Neurology* 43:250–260. <https://doi.org/10.1212/wnl.43.2.250>
135. Kalaria RN, Kenny RA, Ballard CG, Perry R, Ince P, Polvikoski T (2004) Towards defining the neuropathological substrates of vascular dementia. *J Neurol Sci* 226:75–80. <https://doi.org/10.1016/j.jns.2004.09.019>
136. van Straaten EC, Scheltens P, Knol DL et al (2003) Operational definitions for the NINDS-AIREN criteria for vascular dementia: an interobserver study. *Stroke* 34:1907–1912. <https://doi.org/10.1161/01.Str.0000083050.44441.10>
137. Price CC, Jefferson AL, Merino JG, Heilman KM, Libon DJ (2005) Subcortical vascular dementia: integrating neuropsychological and neuroradiologic data. *Neurology* 65:376–382. <https://doi.org/10.1212/01.wnl.0000168877.06011.15>
138. Zhu YC, Tzourio C, Soumaré A, Mazoyer B, Dufouil C, Chabriat H (2010) Severity of dilated Virchow-Robin spaces is associated with age, blood pressure, and MRI markers of small vessel disease: a population-based study. *Stroke* 41:2483–2490. <https://doi.org/10.1161/strokeaha.110.591586>
139. O'Sullivan M, Summers PE, Jones DK, Jarosz JM, Williams SC, Markus HS (2001) Normal-appearing white matter in ischemic leukoaraiosis: a diffusion tensor MRI study. *Neurology* 57:2307–2310. <https://doi.org/10.1212/wnl.57.12.2307>
140. van Norden AG, de Laat KF, van Dijk EJ et al (2012) Diffusion tensor imaging and cognition in cerebral small vessel disease: the RUN DMC study. *Biochim Biophys Acta* 1822:401–407. <https://doi.org/10.1016/j.bbadis.2011.04.008>
141. Fu JL, Zhang T, Chang C, Zhang YZ, Li WB (2012) The value of diffusion tensor imaging in the differential diagnosis of subcortical ischemic vascular dementia and Alzheimer's disease in patients with only mild white matter alterations on T2-weighted images. *Acta Radiol* 53:312–317. <https://doi.org/10.1258/ar.2011.110272>
142. Wang R, Liu N, Tao YY et al (2020) The application of rs-fMRI in vascular cognitive impairment. *Front Neurol* 11:951. <https://doi.org/10.3389/fneur.2020.00951>
143. Kerrouche N, Herholz K, Mielke R, Holthoff V, Baron JC (2006) 18FDG PET in vascular dementia: differentiation from Alzheimer's disease using voxel-based multivariate analysis. *J Cereb Blood Flow Metab* 26:1213–1221. <https://doi.org/10.1038/sj.cbfm.9600296>
144. Pascual B, Prieto E, Arbizu J, Marti-Clement J, Olier J, Masdeu JC (2010) Brain glucose metabolism in vascular white matter disease with dementia: differentiation from Alzheimer disease. *Stroke* 41:2889–2893. <https://doi.org/10.1161/strokeaha.110.591552>
145. Villemagne VL, Ong K, Mulligan RS et al (2011) Amyloid imaging with (18)F-florbetaben in Alzheimer disease and other dementias. *J Nucl Med* 52:1210–1217. <https://doi.org/10.2967/jnumed.111.089730>
146. Lee JH, Kim SH, Kim GH et al (2011) Identification of pure subcortical vascular dementia using 11C-Pittsburgh compound B. *Neurology* 77:18–25. <https://doi.org/10.1212/WNL.0b013e318221acee>
147. Yun HJ, Moon SH, Kim HJ et al (2017) Centiloid method evaluation for amyloid PET of subcortical vascular dementia. *Sci Rep* 7:16322. <https://doi.org/10.1038/s41598-017-16236-1>
148. Ye BS, Seo SW, Kim JH et al (2015) Effects of amyloid and vascular markers on cognitive decline in subcortical vascular dementia. *Neurology* 85:1687–1693. <https://doi.org/10.1212/wnl.0000000000002097>
149. Pluta R, Ulamek-Kozioł M, Januszewski S, Czuczwar SJ (2018) Tau protein dysfunction after brain ischemia. *J Alzheimers Dis* 66:429–437. <https://doi.org/10.3233/jad-180772>
150. Olney NT, Spina S, Miller BL (2017) Frontotemporal dementia. *Neurol Clin* 35:339–374. <https://doi.org/10.1016/j.ncl.2017.01.008>
151. Coyle-Gilchrist IT, Dick KM, Patterson K et al (2016) Prevalence, characteristics, and survival of frontotemporal lobar degeneration syndromes. *Neurology* 86:1736–1743. <https://doi.org/10.1212/wnl.00000000000002638>
152. Knopman DS, Roberts RO (2011) Estimating the number of persons with frontotemporal lobar degeneration in the US population. *J Mol Neurosci* 45:330–335. <https://doi.org/10.1007/s12031-011-9538-y>
153. Pick A (1892) Über die Beziehungen der senilen Hirnatrophie zur Aphasie. *Prager Medizinische Wochenschrift* 17:165–167
154. Rohrer JD, Lashley T, Schott JM et al (2011) Clinical and neuroanatomical signatures of tissue pathology in frontotemporal lobar degeneration. *Brain* 134:2565–2581. <https://doi.org/10.1093/brain/awr198>
155. Goldman JS, Farmer JM, Wood EM et al (2005) Comparison of family histories in FTD subtypes and related tauopathies. *Neurology* 65:1817–1819. <https://doi.org/10.1212/01.wnl.0000187068.92184.63>
156. Lu PH, Mendez MF, Lee GJ et al (2013) Patterns of brain atrophy in clinical variants of frontotemporal lobar degeneration. *Dement Geriatr Cogn Disord* 35:34–50. <https://doi.org/10.1159/000345523>
157. Zhou J, Greicius MD, Gennatas ED et al (2010) Divergent network connectivity changes in behavioural variant frontotemporal dementia and Alzheimer's disease. *Brain* 133:1352–1367. <https://doi.org/10.1093/brain/awq075>
158. Agosta F, Sala S, Valsasina P et al (2013) Brain network connectivity assessed using graph theory in frontotemporal dementia. *Neurology* 81:134–143. <https://doi.org/10.1212/WNL.0b013e31829a33f8>
159. Doppler EG, Rombouts SA, Jiskoot LC et al (2014) Structural and functional brain connectivity in presymptomatic familial frontotemporal dementia. *Neurology* 83:e19–26. <https://doi.org/10.1212/wnl.0000000000000583>
160. Steketee RM, Bron EE, Meijboom R et al (2016) Early-stage differentiation between presenile Alzheimer's disease and frontotemporal dementia using arterial spin labeling MRI. *Eur Radiol* 26:244–253. <https://doi.org/10.1007/s00330-015-3789-x>

161. Salmon E, Garraux G, Delbecq X et al (2003) Predominant ventromedial frontopolar metabolic impairment in frontotemporal dementia. *Neuroimage* 20:435–440. [https://doi.org/10.1016/s1053-8119\(03\)00346-x](https://doi.org/10.1016/s1053-8119(03)00346-x)
162. Kanda T, Ishii K, Uemura T et al (2008) Comparison of grey matter and metabolic reductions in frontotemporal dementia using FDG-PET and voxel-based morphometric MR studies. *Eur J Nucl Med Mol Imaging* 35:2227–2234. <https://doi.org/10.1007/s00259-008-0871-5>
163. Cerami C, Dodich A, Greco L et al (2017) The role of single-subject brain metabolic patterns in the early differential diagnosis of primary progressive aphasia and in prediction of progression to dementia. *J Alzheimers Dis* 55:183–197. <https://doi.org/10.3233/jad-160682>
164. Smith R, Puschmann A, Schöll M et al (2016) 18F-AV-1451 tau PET imaging correlates strongly with tau neuropathology in MAPT mutation carriers. *Brain* 139:2372–2379. <https://doi.org/10.1093/brain/aww163>
165. Spina S, Schonhaut DR, Boeve BF et al (2017) Frontotemporal dementia with the V337M MAPT mutation: Tau-PET and pathology correlations. *Neurology* 88:758–766. <https://doi.org/10.1212/wnl.00000000000003636>
166. Mak E, Nicasastro N, Malpetti M et al (2021) Imaging tau burden in dementia with Lewy bodies using [(18)F]-AV1451 positron emission tomography. *Neurobiol Aging* 101:172–180. <https://doi.org/10.1016/j.neurobiolaging.2020.11.006>
167. Tan RH, Kril JJ, Yang Y et al (2017) Assessment of amyloid β in pathologically confirmed frontotemporal dementia syndromes. *Alzheimers Dement (Amst)* 9:10–20. <https://doi.org/10.1016/j.dadm.2017.05.005>
168. Pringsheim T, Jette N, Frolkis A, Steeves TD (2014) The prevalence of Parkinson's disease: a systematic review and meta-analysis. *Mov Disord* 29:1583–1590. <https://doi.org/10.1002/mds.25945>
169. Wenning GK, Colosimo C, Geser F, Poewe W (2004) Multiple system atrophy. *Lancet Neurol* 3:93–103. [https://doi.org/10.1016/s1474-4422\(03\)00662-8](https://doi.org/10.1016/s1474-4422(03)00662-8)
170. Gilman S, Wenning GK, Low PA et al (2008) Second consensus statement on the diagnosis of multiple system atrophy. *Neurology* 71:670–676. <https://doi.org/10.1212/01.wnl.0000324625.00404.15>
171. Kraft E, Schwarz J, Trenkwalder C, Vogl T, Pfluger T, Oertel WH (1999) The combination of hypointense and hyperintense signal changes on T2-weighted magnetic resonance imaging sequences: a specific marker of multiple system atrophy? *Arch Neurol* 56:225–228. <https://doi.org/10.1001/archneur.56.2.225>
172. Lee WH, Lee CC, Shyu WC, Chong PN, Lin SZ (2005) Hyperintense putaminal rim sign is not a hallmark of multiple system atrophy at 3T. *AJNR Am J Neuroradiol* 26:2238–2242
173. Watanabe H, Saito Y, Terao S et al (2002) Progression and prognosis in multiple system atrophy: an analysis of 230 Japanese patients. *Brain* 125:1070–1083. <https://doi.org/10.1093/brain/awf117>
174. Savoiardo M, Strada L, Girotti F et al (1990) Olivopontocerebellar atrophy: MR diagnosis and relationship to multisystem atrophy. *Radiology* 174:693–696. <https://doi.org/10.1148/radiology.174.3.2305051>
175. Mascalchi M, Vella A, Ceravolo R (2012) Movement disorders: role of imaging in diagnosis. *J Magn Reson Imaging* 35:239–256. <https://doi.org/10.1002/jmri.22825>
176. Rulseh AM, Keller J, Ruzs J et al (2016) Diffusion tensor imaging in the characterization of multiple system atrophy. *Neuropsychiatr Dis Treat* 12:2181–2187. <https://doi.org/10.2147/ndt.S109094>
177. Eckert T, Sailer M, Kaufmann J et al (2004) Differentiation of idiopathic Parkinson's disease, multiple system atrophy, progressive supranuclear palsy, and healthy controls using magnetization transfer imaging. *Neuroimage* 21:229–235
178. Zheng W, Ren S, Zhang H et al (2019) Spatial patterns of decreased cerebral blood flow and functional connectivity in multiple system atrophy (cerebellar-type): a combined arterial spin labeling perfusion and resting state functional magnetic resonance imaging study. *Front Neurosci* 13:777. <https://doi.org/10.3389/fnins.2019.00777>
179. Eckert T, Barnes A, Dhawan V et al (2005) FDG PET in the differential diagnosis of parkinsonian disorders. *Neuroimage* 26:912–921. <https://doi.org/10.1016/j.neuroimage.2005.03.012>
180. Nishimori M, Murata Y, Iwasa H et al (2018) Comparison of MRI and (123)I-FP-CIT SPECT for the evaluation of MSA-P clinical severity. *Biomed Rep* 8:523–528. <https://doi.org/10.3892/br.2018.1086>
181. Litvan I, Agid Y, Jankovic J et al (1996) Accuracy of clinical criteria for the diagnosis of progressive supranuclear palsy (Steele-Richardson-Olszewski syndrome). *Neurology* 46:922–930. <https://doi.org/10.1212/wnl.46.4.922>
182. Dickson DW, Rademakers R, Hutton ML (2007) Progressive supranuclear palsy: pathology and genetics. *Brain Pathol* 17:74–82. <https://doi.org/10.1111/j.1750-3639.2007.00054.x>
183. Kato N, Arai K, Hattori T (2003) Study of the rostral midbrain atrophy in progressive supranuclear palsy. *J Neurol Sci* 210:57–60. [https://doi.org/10.1016/s0022-510x\(03\)00014-5](https://doi.org/10.1016/s0022-510x(03)00014-5)
184. Seppi K, Poewe W (2010) Brain magnetic resonance imaging techniques in the diagnosis of parkinsonian syndromes. *Neuroimaging Clin N Am* 20:29–55. <https://doi.org/10.1016/j.nic.2009.08.016>
185. Spoto N, Hall S, Irwin DJ et al (2019) Diffusion tensor MRI to distinguish progressive supranuclear palsy from α -synucleinopathies. *Radiology* 293:646–653. <https://doi.org/10.1148/radiol.2019190406>
186. Bharti K, Bologna M, Upadhyay N et al (2017) Abnormal resting-state functional connectivity in progressive supranuclear palsy and corticobasal syndrome. *Front Neurol* 8:248. <https://doi.org/10.3389/fneur.2017.00248>
187. Brendel M, Barthel H, van Eimeren T et al (2020) Assessment of 18F-PI-2620 as a biomarker in progressive supranuclear palsy. *JAMA Neurol* 77:1408–1419. <https://doi.org/10.1001/jamaneurol.2020.2526>
188. Vaar AM, de Nijs T, Kessels AG et al (2008) Diagnostic value of 123I-ioflupane and 123I-iodobenzamide SPECT scans in 248 patients with parkinsonian syndromes. *Eur Neurol* 59:258–266. <https://doi.org/10.1159/000115640>
189. Brooks DJ (2002) Diagnosis and management of atypical parkinsonian syndromes. *J Neurol Neurosurg Psychiatry* 72(Suppl 1):i10–i16. https://doi.org/10.1136/jnnp.72.suppl_1.i10
190. Lee SE, Rabinovici GD, Mayo MC et al (2011) Clinicopathological correlations in corticobasal degeneration. *Ann Neurol* 70:327–340. <https://doi.org/10.1002/ana.22424>
191. Dickson DW, Bergeron C, Chin SS et al (2002) Office of rare diseases neuropathologic criteria for corticobasal degeneration. *J Neuropathol Exp Neurol* 61:935–946. <https://doi.org/10.1093/jnen/61.11.935>
192. Koyama M, Yagishita A, Nakata Y, Hayashi M, Bando M, Mizutani T (2007) Imaging of corticobasal degeneration syndrome. *Neuroradiology* 49:905–912. <https://doi.org/10.1007/s00234-007-0265-6>
193. Erbetta A, Mandelli ML, Savoiardo M et al (2009) Diffusion tensor imaging shows different topographic involvement of the thalamus in progressive supranuclear palsy and corticobasal degeneration. *AJNR Am J Neuroradiol* 30:1482–1487. <https://doi.org/10.3174/ajnr.A1615>
194. Teune LK, Bartels AL, de Jong BM et al (2010) Typical cerebral metabolic patterns in neurodegenerative brain diseases. *Mov Disord* 25:2395–2404. <https://doi.org/10.1002/mds.23291>
195. Mille E, Levin J, Brendel M et al (2017) Cerebral glucose metabolism and dopaminergic function in patients with corticobasal syndrome. *J Neuroimaging* 27:255–261. <https://doi.org/10.1111/jon.12391>
196. Josephs KA, Whitwell JL, Tacik P et al (2016) [18F]AV-1451 tau-PET uptake does correlate with quantitatively measured 4R-tau burden in autopsy-confirmed corticobasal degeneration. *Acta Neuropathol* 132:931–933. <https://doi.org/10.1007/s00401-016-1618-1>
197. Lowe VJ, Curran G, Fang P et al (2016) An autoradiographic evaluation of AV-1451 Tau PET in dementia. *Acta Neuropathol Commun* 4:58. <https://doi.org/10.1186/s40478-016-0315-6>
198. Palleis C, Brendel M, Finze A et al (2021) Cortical [(18)F]PI-2620 binding differentiates corticobasal syndrome subtypes. *Mov Disord* 36:2104–2115. <https://doi.org/10.1002/mds.28624>
199. Pirker W, Asenbaum S, Bencsits G et al (2000) [123I]beta-CIT SPECT in multiple system atrophy, progressive supranuclear palsy, and corticobasal degeneration. *Mov Disord* 15:1158–1167. [https://doi.org/10.1002/1531-8257\(200011\)15:6%3c1158::aid-mds1015%3e3.0.co;2-0](https://doi.org/10.1002/1531-8257(200011)15:6%3c1158::aid-mds1015%3e3.0.co;2-0)
200. Badoud S, Van De Ville D, Nicasastro N, Garibotto V, Burkhard PR, Haller S (2016) Discriminating among degenerative parkinsonisms using advanced (123)I-ioflupane SPECT analyses. *Neuroimage Clin* 12:234–240. <https://doi.org/10.1016/j.nicl.2016.07.004>
201. Pantelakis S (1954) A particular type of senile angiopathy of the central nervous system: congophilic angiopathy, topography and frequency. *Monatsschr Psychiatr Neurol* 128:219–256
202. Biffi A, Rosenberg SM (2011) Cerebral amyloid angiopathy: a systematic review. *J Clin Neurol* 7:1–9. <https://doi.org/10.3988/jcn.2011.7.1.1>

203. Jellinger KA (2002) Alzheimer disease and cerebrovascular pathology: an update. *J Neural Transm (Vienna)* 109:813–836. <https://doi.org/10.1007/s007020200068>
204. Charidimou A, Boulouis G, Frosch MP et al (2022) The Boston criteria version 2.0 for cerebral amyloid angiopathy: a multicentre, retrospective, MRI-neuropathology diagnostic accuracy study. *Lancet Neurol* 21:714–725. [https://doi.org/10.1016/s1474-4422\(22\)00208-3](https://doi.org/10.1016/s1474-4422(22)00208-3)
205. Miller-Thomas MM, Sipe AL, Benzinger TL, McConathy J, Connolly S, Schwetye KE (2016) Multimodality review of amyloid-related diseases of the central nervous system. *Radiographics* 36:1147–1163. <https://doi.org/10.1148/rg.2016150172>
206. Baron JC, Farid K, Dolan E et al (2014) Diagnostic utility of amyloid PET in cerebral amyloid angiopathy-related symptomatic intracerebral hemorrhage. *J Cereb Blood Flow Metab* 34:753–758. <https://doi.org/10.1038/jcbfm.2014.43>
207. Farid K, Hong YT, Aigbirhio FI et al (2015) Early-phase 11C-PiB PET in amyloid angiopathy-related symptomatic cerebral hemorrhage: potential diagnostic value? *PLoS One* 10:e0139926. <https://doi.org/10.1371/journal.pone.0139926>
208. Charidimou A, Farid K, Tsai HH, Tsai LK, Yen RF, Baron JC (2018) Amyloid-PET burden and regional distribution in cerebral amyloid angiopathy: a systematic review and meta-analysis of biomarker performance. *J Neurol Neurosurg Psychiatry* 89:410–417. <https://doi.org/10.1136/jnnp-2017-316851>
209. Bergeret S, Queneau M, Rodalleg M et al (2021) [(18)F]FDG PET may differentiate cerebral amyloid angiopathy from Alzheimer's disease. *Eur J Neurol* 28:1511–1519. <https://doi.org/10.1111/ene.14743>
210. Schoemaker D, Charidimou A, Zanon Zotin MC et al (2021) Association of memory impairment with concomitant tau pathology in patients with cerebral amyloid angiopathy. *Neurology* 96:e1975–e1986. <https://doi.org/10.1212/wnl.00000000000011745>
211. Roberts GW, Allsop D, Bruton C (1990) The occult aftermath of boxing. *J Neurol Neurosurg Psychiatry* 53:373–378. <https://doi.org/10.1136/jnnp.53.5.373>
212. McKee AC, Cantu RC, Nowinski CJ et al (2009) Chronic traumatic encephalopathy in athletes: progressive tauopathy after repetitive head injury. *J Neuropathol Exp Neurol* 68:709–735. <https://doi.org/10.1097/NEN.0b013e3181a9d503>
213. McKee AC, Stern RA, Nowinski CJ et al (2013) The spectrum of disease in chronic traumatic encephalopathy. *Brain* 136:43–64. <https://doi.org/10.1093/brain/aww307>
214. Koerte IK, Hufschmidt J, Muehlmann M et al (2016) Cavum septi pellucidi in symptomatic former professional football players. *J Neurotrauma* 33:346–353. <https://doi.org/10.1089/neu.2015.3880>
215. Bang SA, Song YS, Moon BS et al (2016) Neuropsychological, metabolic, and GABAA receptor studies in subjects with repetitive traumatic brain injury. *J Neurotrauma* 33:1005–1014. <https://doi.org/10.1089/neu.2015.4051>
216. Multani N, Goswami R, Khodadadi M et al (2016) The association between white-matter tract abnormalities, and neuropsychiatric and cognitive symptoms in retired professional football players with multiple concussions. *J Neurol* 263:1332–1341. <https://doi.org/10.1007/s00415-016-8141-0>
217. Wilde EA, Hunter JV, Li X et al (2016) Chronic effects of boxing: diffusion tensor imaging and cognitive findings. *J Neurotrauma* 33:672–680. <https://doi.org/10.1089/neu.2015.4035>
218. Mayer AR, Ling JM, Dodd AB, Meier TB, Hanlon FM, Klimaj SD (2017) A prospective microstructure imaging study in mixed-martial artists using geometric measures and diffusion tensor imaging: methods and findings. *Brain Imaging Behav* 11:698–711. <https://doi.org/10.1007/s11682-016-9546-1>
219. Stern RA, Adler CH, Chen K et al (2019) Tau positron-emission tomography in former national football league players. *N Engl J Med* 380:1716–1725. <https://doi.org/10.1056/NEJMoa1900757>
220. Lesman-Segev OH, La Joie R, Stephens ML et al (2019) Tau PET and multimodal brain imaging in patients at risk for chronic traumatic encephalopathy. *Neuroimage Clin* 24:102025. <https://doi.org/10.1016/j.nicl.2019.102025>
221. Masrori P, Van Damme P (2020) Amyotrophic lateral sclerosis: a clinical review. *Eur J Neurol* 27:1918–1929. <https://doi.org/10.1111/ene.14393>
222. Neumann M, Sampathu DM, Kwong LK et al (2006) Ubiquitinated TDP-43 in frontotemporal lobar degeneration and amyotrophic lateral sclerosis. *Science* 314:130–133. <https://doi.org/10.1126/science.1134108>
223. Comi G, Rovaris M, Leocani L (1999) Review neuroimaging in amyotrophic lateral sclerosis. *Eur J Neurol* 6:629–637. <https://doi.org/10.1046/j.1468-1331.1999.660629.x>
224. Hecht MJ, Fellner F, Fellner C, Hilz MJ, Heuss D, Neundörfer B (2001) MRI-FLAIR images of the head show corticospinal tract alterations in ALS patients more frequently than T2-, T1- and proton-density-weighted images. *J Neurol Sci* 186:37–44. [https://doi.org/10.1016/s0022-510x\(01\)00503-2](https://doi.org/10.1016/s0022-510x(01)00503-2)
225. Jin J, Hu F, Zhang Q, Jia R, Dang J (2016) Hyperintensity of the corticospinal tract on FLAIR: a simple and sensitive objective upper motor neuron degeneration marker in clinically verified amyotrophic lateral sclerosis. *J Neurol Sci* 367:177–183. <https://doi.org/10.1016/j.jns.2016.06.005>
226. Foerster BR, Carlos RC, Dwamena BA et al (2014) Multimodal MRI as a diagnostic biomarker for amyotrophic lateral sclerosis. *Ann Clin Transl Neurol* 1:107–114. <https://doi.org/10.1002/acn3.30>
227. Cheong I, Marjańska M, Deelchand DK, Eberly LE, Walk D, Öz G (2017) Ultra-high field proton MR spectroscopy in early-stage amyotrophic lateral sclerosis. *Neurochem Res* 42:1833–1844. <https://doi.org/10.1007/s11064-017-2248-2>
228. Costagli M, Donatelli G, Biagi L et al (2016) Magnetic susceptibility in the deep layers of the primary motor cortex in amyotrophic lateral sclerosis. *Neuroimage Clin* 12:965–969. <https://doi.org/10.1016/j.nicl.2016.04.011>
229. Zhou F, Gong H, Li F et al (2013) Altered motor network functional connectivity in amyotrophic lateral sclerosis: a resting-state functional magnetic resonance imaging study. *NeuroReport* 24:657–662. <https://doi.org/10.1097/WNR.0b013e328363148c>
230. Van Laere K, Vanhee A, Verschueren J et al (2014) Value of 18fluoro-deoxyglucose-positron-emission tomography in amyotrophic lateral sclerosis: a prospective study. *JAMA Neurol* 71:553–561. <https://doi.org/10.1001/jamaneuro.2014.62>
231. Paganì M, Chiò A, Valentini MC et al (2014) Functional pattern of brain FDG-PET in amyotrophic lateral sclerosis. *Neurology* 83:1067–1074. <https://doi.org/10.1212/wnl.0000000000000792>
232. Shinotoh H, Shimada H, Kokubo Y et al (2019) Tau imaging detects distinctive distribution of tau pathology in ALS/PDC on the Kii Peninsula. *Neurology* 92:e136–e147. <https://doi.org/10.1212/wnl.0000000000006736>
233. McColgan P, Tabrizi SJ (2018) Huntington's disease: a clinical review. *Eur J Neurol* 25:24–34. <https://doi.org/10.1111/ene.13413>
234. Tabrizi SJ, Scahill RI, Owen G et al (2013) Predictors of phenotypic progression and disease onset in premanifest and early-stage Huntington's disease in the TRACK-HD study: analysis of 36-month observational data. *Lancet Neurol* 12:637–649. [https://doi.org/10.1016/s1474-4422\(13\)70088-7](https://doi.org/10.1016/s1474-4422(13)70088-7)
235. Estevez-Fraga C, Scahill R, Rees G, Tabrizi SJ, Gregory S (2020) Diffusion imaging in Huntington's disease: comprehensive review. *J Neurol Neurosurg Psychiatry* 92:62–69. <https://doi.org/10.1136/jnnp-2020-324377>
236. Ciarmiello A, Cannella M, Lasteria S et al (2006) Brain white-matter volume loss and glucose hypometabolism precede the clinical symptoms of Huntington's disease. *J Nucl Med* 47:215–222
237. Andrews TC, Weeks RA, Turjanski N et al (1999) Huntington's disease progression. PET and clinical observations. *Brain* 122(Pt 12):2353–2363. <https://doi.org/10.1093/brain/122.12.2353>
238. Cybulska K, Perk L, Boonij J, Laverman P, Rijpkema M (2020) Huntington's disease: a review of the known PET imaging biomarkers and targeting radiotracers. *Molecules*. <https://doi.org/10.3390/molecules25030482>
239. Uttley L, Carroll C, Wong R, Hilton DA, Stevenson M (2020) Creutzfeldt-Jakob disease: a systematic review of global incidence, prevalence, infectivity, and incubation. *Lancet Infect Dis* 20:e2–e10. [https://doi.org/10.1016/s1473-3099\(19\)30615-2](https://doi.org/10.1016/s1473-3099(19)30615-2)
240. Fragoso DC, Gonçalves Filho AL, Pacheco FT et al (2017) Imaging of Creutzfeldt-Jakob disease: imaging patterns and their differential diagnosis. *Radiographics* 37:234–257. <https://doi.org/10.1148/rg.2017.60075>

241. Tschampa HJ, Kallenberg K, Urbach H et al (2005) MRI in the diagnosis of sporadic Creutzfeldt-Jakob disease: a study on inter-observer agreement. *Brain* 128:2026–2033. <https://doi.org/10.1093/brain/awh575>
242. Galanaud D, Haik S, Linguraru MG et al (2010) Combined diffusion imaging and MR spectroscopy in the diagnosis of human prion diseases. *AJNR Am J Neuroradiol* 31:1311–1318. <https://doi.org/10.3174/ajnr.A2069>
243. Kim EJ, Cho SS, Jeong BH et al (2012) Glucose metabolism in sporadic Creutzfeldt-Jakob disease: a statistical parametric mapping analysis of (18) F-FDG PET. *Eur J Neurol* 19:488–493. <https://doi.org/10.1111/j.1468-1331.2011.03570.x>
244. Renard D, Castelnovo G, Collombier L, Thouvenot E, Boudousq V (2017) FDG-PET in Creutzfeldt-Jakob disease: analysis of clinical-PET correlation. *Prion* 11:440–453. <https://doi.org/10.1080/19336896.2017.1387348>
245. Villemagne VL, McLean CA, Reardon K et al (2009) 11C-PIB PET studies in typical sporadic Creutzfeldt-Jakob disease. *J Neurol Neurosurg Psychiatry* 80:998–1001. <https://doi.org/10.1136/jnnp.2008.171496>
246. Matias-Guiu JA, Guerrero-Márquez C, Cabrera-Martín MN et al (2017) Amyloid- and FDG-PET in sporadic Creutzfeldt-Jakob disease: correlation with pathological prion protein in neuropathology. *Prion* 11:205–213. <https://doi.org/10.1080/19336896.2017.1314427>
247. Day GS, Gordon BA, Perrin RJ et al (2018) In vivo [(18)F]-AV-1451 tau-PET imaging in sporadic Creutzfeldt-Jakob disease. *Neurology* 90:e896–e906. <https://doi.org/10.1212/wnl.0000000000005064>
248. Kim HJ, Cho H, Park S et al (2019) THK5351 and flortaucipir PET with pathological correlation in a Creutzfeldt-Jakob disease patient: a case report. *BMC Neurol* 19:211. <https://doi.org/10.1186/s12883-019-1434-z>
249. Kiloh LG (1961) Pseudo-dementia. *Acta Psychiatr Scand* 37:336–351. <https://doi.org/10.1111/j.1600-0447.1961.tb07367.x>
250. Small GW, Liston EH, Jarvik LF (1981) Diagnosis and treatment of dementia in the aged. *West J Med* 135:469–481
251. Yesavage JA, Brink TL, Rose TL et al (1982) Development and validation of a geriatric depression screening scale: a preliminary report. *J Psychiatr Res* 17:37–49. [https://doi.org/10.1016/0022-3956\(82\)90033-4](https://doi.org/10.1016/0022-3956(82)90033-4)
252. Rasgon NL, Kenna HA, Geist C, Small G, Silverman D (2008) Cerebral metabolic patterns in untreated postmenopausal women with major depressive disorder. *Psychiatry Res* 164:77–80. <https://doi.org/10.1016/j.psychres.2007.12.006>
253. Loreto F, Gunning S, Golemme M et al (2021) Evaluating cognitive profiles of patients undergoing clinical amyloid-PET imaging. *Brain Commun* 3:fcab035. <https://doi.org/10.1093/braincomms/fcab035>

Publisher's Note

Springer Nature remains neutral with regard to jurisdictional claims in published maps and institutional affiliations.

Submit your manuscript to a SpringerOpen[®] journal and benefit from:

- Convenient online submission
- Rigorous peer review
- Open access: articles freely available online
- High visibility within the field
- Retaining the copyright to your article

Submit your next manuscript at ► [springeropen.com](https://www.springeropen.com)
